Faculty of Medicine and Life Sciences
School for Life Sciences
Master of Biomedical Sciences

Master's thesis

Gap junction intercellular communication in suicide gene therapy for oral squamous cell carcinoma: an in vitro study

Kim Nijsten

Thesis presented in fulfillment of the requirements for the degree of Master of Biomedical Sciences, specialization Molecular Mechanisms in Health and Disease

SUPERVISOR :
Prof. dr. Esther WOLFS

MENTOR :
Mevrouw Jolien VAN DEN BOSCH

2020
2021

Faculty of Medicine and Life Sciences
School for Life Sciences

Master of Biomedical Sciences

Master's thesis

Gap junction intercellular communication in suicide gene therapy for oral squamous cell carcinoma: an in vitro study

Kim Nijsten

Thesis presented in fulfillment of the requirements for the degree of Master of Biomedical Sciences, specialization Molecular Mechanisms in Health and Disease

SUPERVISOR :
Prof. dr. Esther WOLFS

MENTOR :
Mevrouw Jolien VAN DEN BOSCH

Gap junction intercellular communication in suicide gene therapy for oral squamous cell carcinoma: an *in vitro* study*

Kim Nijsten[1], Jolien Van Den Bosch[1], Ivo Lambrichts[1], and Esther Wolfs[1]

[1]Biomedical Research institute, Universiteit Hasselt, Campus Diepenbeek, Agoralaan Gebouw C - B-3590 Diepenbeek

*Running title: *A stem cell-based suicide gene therapy for OSCC*

To whom correspondence should be addressed: Esther Wolfs, Tel: +32 (11) 26 92 96; Email: esther.wolfs@uhasselt.be

Keywords: OSCC, stem cell-based therapy, DPSC, HSV1-TK/GCV system, gap junction intercellular communication

ABSTRACT

Oral squamous cell carcinoma (OSCC) is the most common type of head and neck cancer. Current treatment approaches include radiotherapy, chemotherapy, and surgery. Nevertheless, severe discomfort and side effects are often observed following these treatments. Hence, we strive to establish an alternative treatment strategy preserving the healthy tissue by selectively targeting the tumor via a stem cell-based suicide gene therapy. In this project, we aim to validate the role of the gap junction intercellular communication (GJIC) between human dental pulp stem cells (DPSC) and OSCC cells as this mechanism is proposed to ensure a successful therapy. Moreover, the Herpes Simplex Virus 1 thymidine kinase (HSV1-TK)/ganciclovir (GCV) system and DPSC as the carrier of the suicide gene therapy will be evaluated *in vitro*. Immunocytochemistry demonstrated connexin 43 expression in the DPSC/OSCC co-culture model. Moreover, a Lucifer Yellow dye-transfer assay was performed to evaluate the gap junction functionality. Here, transfer of Lucifer Yellow to adjacent cells at cell-dense regions was observed, suggesting functionally active gap junctions. Lastly, primary data obtained from GCV administration to HSV1-TK-expressing cells demonstrated a first indication of the system's cytotoxic success *in vitro*. In summary, our preliminary data support the role of GJIC in the co-culture model and pose promising results indicating the potency of the HSV1-TK/GCV system in a stem cell-based setting. However, additional research is required to validate and strengthen preliminary results as well as the usage of DPSC in suicide gene therapy for OSCC.

1. Oral squamous cell carcinoma

The broad term cancer describes a group of neoplastic diseases responsible for significant morbidity and mortality worldwide (1, 2). A multistep development characterizes the pathogenesis of cancer summarized into six primary hallmarks: (1) maintenance of proliferative signaling, (2) uncontrolled, chronic cell proliferation, (3) growth suppressing insensitivity, (4) avoidance of apoptosis, (5) induction of angiogenesis, and (6) triggering of invasion and metastasis. These altered cell capabilities facilitate normal cells to convert into tumorigenic and, eventually, malignant cell masses. Moreover, both genome instability and inflammation underlie and promote these acquired functions. Additionally, the latest research suggests two emerging cancer cell features that enable the cells to dysregulate their cellular energy metabolism and also to avoid elimination by the host's immune system. Furthermore, recent findings imply that not only the tumor cells themself have an impact on the tumorigenesis, but also its surrounding environment. This microenvironment is established and continually changing during this complex multistep process of tumor development. Moreover, it is able to influence this process via reciprocal signaling between, e.g., the stromal or parenchymal cells and the tumor cells (2). In addition, various external factors, such as chemical

carcinogens, electromagnetic radiation, dietary components, infectious and immunosuppressive agents, etc., can cause cell abnormality and contribute to tumor formation (3).

Specifically, head and neck cancer (HNC) is described as heterogeneous tumors that manifest in the oral or sinonasal cavity, larynx, pharynx, or nasopharynx (4-6). With 890 000 new cases and approximately 450 000 deaths annually, HNC is the seventh most common cancer type worldwide (1, 4). Older people (50-66 years old), where men are at higher risk than women, represent the average patient profile for HNC (1, 5, 7). Moreover, the World Health Organization has determined various factors that increase the HNC risk like alcohol and tobacco consumption, viral infections (e.g., Human Papilloma Virus (HPV), Ebstein Barr Virus (EBV)), and environmental toxins (5, 7-9).

This study focuses on squamous cell carcinomas formed in the oral cavity (OSCC). Its epidemiology, pathology, and treatment options however are similar to the other types of HNC (4). Most malignancies occurring in these regions arise from the lining of soft mucosal tissue known as squamous cell carcinomas (4-6). Its pathophysiological development starts with hyperplasia of the epithelial cells. Subsequently, dysplasia or abnormal cell development occurs, followed by carcinoma in situ, which results in an aggressive tumor (5). Clinical indications for OSCC, which are difficult to observe in an early phase, include a burning feeling, leukoplakia, erythroplakia, and an ulcer-like appearance (7).

The prognosis and treatment strategy depends on the tumors location, stage, and epidemiologic aspects (4). Current therapies include surgery, chemotherapy, radiotherapy, or a combination (7, 9). Even though the therapy options have improved over the years, the 5-year survival rate still remains approximately 50% (7). Additionally, the patients might experience severe discomfort following treatment, like eating and drinking difficulties, speaking problems, missing facial parts, etc. (9). Therefore, it is crucial to search for alternative treatment strategies that improve the survival rate and enhance the patients' quality of life. This study will attempt to reach these goals by eliminating the tumor cells selectively while minimizing harm to the surrounding healthy tissue via a stem cell-based suicide gene therapy.

2. Stem cell-based suicide gene therapy
Suicide gene therapy

Due to the development of *in vivo* and *ex vivo* gene delivery systems, as well as the growing clinical knowledge concerning this approach, gene therapy became an attractive alternative for conventional cancer treatments (10-13). Here, a long-lasting, stable expression of a therapeutic or transgene is desired to improve or even cure disease-associated symptoms while minimizing adverse effects. Moreover, successful outcomes have been reported for a number of cancers as well as a variety of genetic disorders such as sickle cell disease (12, 14).

Gene therapy in the cancer field can be categorized into three subclasses: (1) correcting, (2) toxin/apoptosis-inducing, and (3) suicide gene therapy. In the first class, the therapeutic gene is implemented to correct the disturbed gene profile halting the unrestricted proliferation capacity of the tumor cells. The second approach, on the other hand, involves the production of cytotoxic proteins that are desired to cause apoptosis in the transduced cells. Although their principle is very promising, both strategies experience the same limitation: only cells in which the therapeutic gene is introduced will be affected. This results in the failure to eliminate all tumor cells while simultaneously allowing further proliferation of the residual cells. The last category, however, entails a two-step strategy to overcome the previously mentioned drawbacks (11). The principle suicide gene therapy or gene-directed enzyme prodrug therapy (GDEPT) is a therapeutic approach based on the transfer of a suicide gene in tumor cells. This gene encodes an enzyme that is able to convert a prodrug into its active pharmacological variant, resulting in cell death (15, 16). Thereby, it establishes high cytotoxicity in the tumor tissue while keeping the damage to the surrounding environment to a minimum (11). The great interest in this approach can be allocated to the extension of the cytotoxic effect to neighboring cells resulting in a larger killing zone. This phenomenon is referred to as the bystander effect, on which the success of this therapeutic approach highly depends (11, 15, 16). Furthermore, the enzyme, prodrug and delivery system of choice play an important role considering their safety issues, therapeutic efficiency, and success when working towards the clinical implementation of the therapy (11).

2

There are two well-known and widely studied suicide gene/prodrug systems: (1) Herpes Simplex Virus 1 thymidine kinase (HSV1-TK)/ganciclovir (GCV), and (2) cytosine deaminase (CD)/5-fluorocytosine. The suicide gene HSV1-TK can phosphorylate pyrimidine and purine, as well as their analogs. First, GCV is phosphorylated by this suicide gene into a monophosphate (GCV-P), and thereafter further metabolization to GCV triphosphate (GCV-3P) by intracellular enzymes is observed. Subsequently, GCV will exert its cytotoxic effect by incorporating into the cell's DNA, leading to single-stranded breaks as well as causing cell cycle blockage, eventually resulting in cell death (16-19). Several advantages are associated with this suicide gene/prodrug system. First of all, since GCV-3P is only able to incorporate into the replicating DNA strand and does not hinder eukaryotic DNA polymerase, it is just lethal to dividing cells. Moreover, this establishes a very beneficial advantage because, as mentioned before, cancer cells are in an uncontrolled and chronic proliferation state (15). However, this also limits this therapy to dividing cells only (16). Secondly, HSV1-TK can phosphorylate GCV far more efficiently than its cellular equivalent thymidine, implying that it will cause little toxicity in non-transduced cells (15). Despite HSV1-TK's superior affinity for GCV compared to its biological substrate thymidine, a very high GCV dosage is still required for the drug to attain its spot at the active site. This high GCV dose often leads to off-target toxicity, causing e.g. serious immune and bone marrow suppression (11, 16, 20, 21). Therefore, researchers tackled this issue by modifying the active site of the HSV1-TK gene resulting in a variety of HSV1-TK mutants (11, 22, 23). Black et al. demonstrated that the SR39 modified HSV1-TK variant, which is used in this project, could metabolize GCV more efficiently. Even when the GCV dosage decreased with 294 fold an effect was observed by this mutant, while no response from wild-type HSV1-TK was noticed (22). Additionally, another obstacle is the therapy's high dependence on the intercellular gap junction communication between cells for the transportation of the entrapped toxic metabolite since this mechanism is often impaired in cancer tissue (16, 24, 25).

Such as HSV1-TK, CD deaminates the non-toxic 5-fluorocytosine into 5-fluorouracil, which is a very potent chemotherapeutic agent in cancer treatment (15, 16). However, significant adverse events are related to its therapeutic dosage, such as cardiac toxicity (16). Because both the enzyme and substrate are commonly used in a clinical setting, and the potential side effects are well-identified, clinical trials using this approach are more easily facilitated. Yet, only limited success has been documented concerning trials testing this strategy (15).

Gene delivery

In gene therapy, the transfer of therapeutic genes can be accomplished via two fundamental approaches. The gene can either be transferred into the cell via a non-integrated vector or an integrating vector. The first strategy involves post- or slowly dividing cells in which the transgene expression is generated and remains for the cell's lifetime. The other indirect approach is based on the establishment of expression in a precursor or stem cell. Due to the integration of the vector, the gene is passed through to daughter cells when dividing (14). For the application of gene delivery systems as a component in cancer therapy, several characteristics are desired: (1) high transfection efficiency of the inserted gene, (2) minimal cytotoxicity in the targeted tissue, (3) low immunogenicity, (4) high tissue specificity, (5) cost-effectivity. In addition, three major categories of gene delivery systems can be distinguished: (1) microorganism-based, (2) synthetic, or (3) cell-based. The first category involves bacterial, viral, and yeast-based systems (11). Examples of commonly studied viral vectors are adenoviral vectors, retroviral/lentiviral vectors, and adeno-associated viruses (12, 16). Adenoviral vectors are to date the preferred gene delivery system in the clinical phase. Despite the (pre)clinical success due to their beneficial characteristics, such as transfection of dividing and non-dividing cells, several drawbacks like clearance of the viral particles and high immunogenicity limit their success in clinical trials (11). In contrast to adenoviral vectors, lentiviral vectors can achieve long-lasting expression of the transgene by integrating it into the host's genome. Moreover, they usually do not evoke a significant immune response, in contrast to adenoviral vectors (11, 12, 16). However, the major drawback of lentiviral gene delivery is the higher risk of insertional

mutagenesis, which needs to be further investigated (11). Secondly, synthetic vectors such as cationic polymers and liposomes do not achieve the same gene delivery efficiency. Moreover, their safety and toxicity issues have to be resolved (12, 15, 26). Lastly, various cell types, such as dendritic cells and stem cells, can be employed in cell-based delivery systems. Instead of administering the viral or non-viral delivery systems directly to target the tumor, other cells are ex vivo engineered to express the gene of interest and/or antigens before their application as a delivery system (27). In our study, a cell-based gene delivery will be applied. More specifically, we aim to employ dental pulp stem cells, a subtype of the mesenchymal stem cell family, as a gene delivery system of the HSV1-TK suicide gene.

Gap junction intercellular communication

To extend the therapeutic effect of the suicide gene therapy to non-transduced cells, it is highly depending on the bystander killing mechanism. As mentioned before, this phenomenon involves the expansion of the toxic effect initiated in the suicide gene expressing cells to the neighboring ones. More specifically, the prodrug also eliminates non-transduced cells after metabolization by the suicide gene and exchange of its toxic form to adjacent cells (11, 15, 16). Several mechanisms can be responsible for transferring the metabolized prodrug. A first mechanism involves apoptotic bodies that are released from dying cells which will then be endocytosed by adjacent cells. Secondly, upon activation of the immune system, a distant bystander effect can be triggered, meaning that events occurring at the primary tumor site can prevent the formation of metastatic tumors. Finally, the extension of the cytotoxic effect can be caused by passive diffusion, according through their concentration gradient, or active diffusion via gap junction intercellular communication due to the small size of most prodrugs (11).

The formation of gap junctions occurs when connexons or hemichannels present in the plasma membranes of neighboring cells adhere allowing direct cell communication. Furthermore, these hemichannels consist of 6 transmembrane connexin subunits, which can vary in composition of connexin types. Up until this moment, 21 different types are known to be present in the human genome, of which connexin 43 (Cx43) is the most predominantly expressed connexin in mammalian cells (28, 29). Moreover, Cx43 expression is also correlated with the prognosis of oral squamous cell carcinoma. In dysplasia-free regions, Cx43 expression might indicate primary tumor development in a very early state (30).

The role of stem cells in gene therapy

The group of *Miletic et al.* investigated the HSV1-TK/GCV-based therapy using bone marrow-derived progenitor cells (BM-MSC) as a vehicle for suicide gene therapy to treat malignant gliomas. Here, the bystander effect was established by gap junctional intercellular communication (GJIC) between the cells. In other words, GCV was transferred from the BM-MSCs to the tumor cells through gap junctions achieving a successful outcome (31). Over the past decades, research has investigated the role of stem cells as a vehicle for gene therapy. A stem cell has self-renewal capacities as well as the ability to differentiate to various cell lineages depending on its nature (32). Pluripotent embryonic stem cells and multipotent adult stem cells are two well-described stem cell types (33, 34). The greatest benefit of embryonic stem cells is their pluripotency, meaning they are able to differentiate into cell types of all three embryonic layers. However, ethical and political controversies are associate with their use, and there is a high risk of the formation of teratomas (35, 36). (36). Finally, adult stem cells are present in the body to repair damaged tissue due to their multipotent self-renewable capacity. They reside in a specialized compartment called a stem cell niche, which ensures, for example, their proliferation, and prevents its exhaustion. Mesenchymal stem cells (MSCs) are adult stem cells isolated from several niches, such as the bone marrow (33). For a stem cell to be classified as an MSC, the *Mesenchymal and Tissue Stem Cell Committee of the International Society for Cellular Therapy (ISCT MSC)* determined several criteria that must be met: (1) plastic-adherent, (2) specific surface marker expression (CD73, CD90, CD105), (3) lack of surface expression of CD11b or CD14, CD19 or CD79a, CD34, CD45, and HLA-DR, and (4) a trilineage - chondrogenic, osteogenic, and adipogenic - differentiation potential (33, 37).

Additionally, MSC-like cells matching these criteria can also be isolated from dental pulp, referred to as dental pulp stem cells (DPSC). Furthermore, DPSC have several advantages compared to other MSC-subtypes. First, their isolation is easier because they are extracted from a waste product of orthodontic surgery. Therefore, limited ethical issues are present. Secondly, they can be cryopreserved and stored for a long time without losing their valuable stem cell capabilities (33). Furthermore, they also possess two features beneficial for this study: (1) tumor tropism /migration and (2) immunomodulation capacity (38, 39). More specifically, Merckx et al. demonstrated the tumor homing capability of DPSC *in vitro* (40). Furthermore, the group of Howard C. showed that sphingosine-1-phosphate (S1P) as well as laminin induced a more extensive migration of the DPSC compared to other chemoattractant and extracellular matrix proteins (41). Moreover, they are capable of suppressing any immune reaction, which enables their protection from elimination after administration (38, 39).

In this study, we will employ the HSV1-TK/GCV system as the mechanism of action for the suggested suicide gene therapy. **Fig. 1** provides a summary of the therapy principle. Additionally, we will evaluate DPSC as a vehicle for suicide gene therapy. Currently, limited is known on their
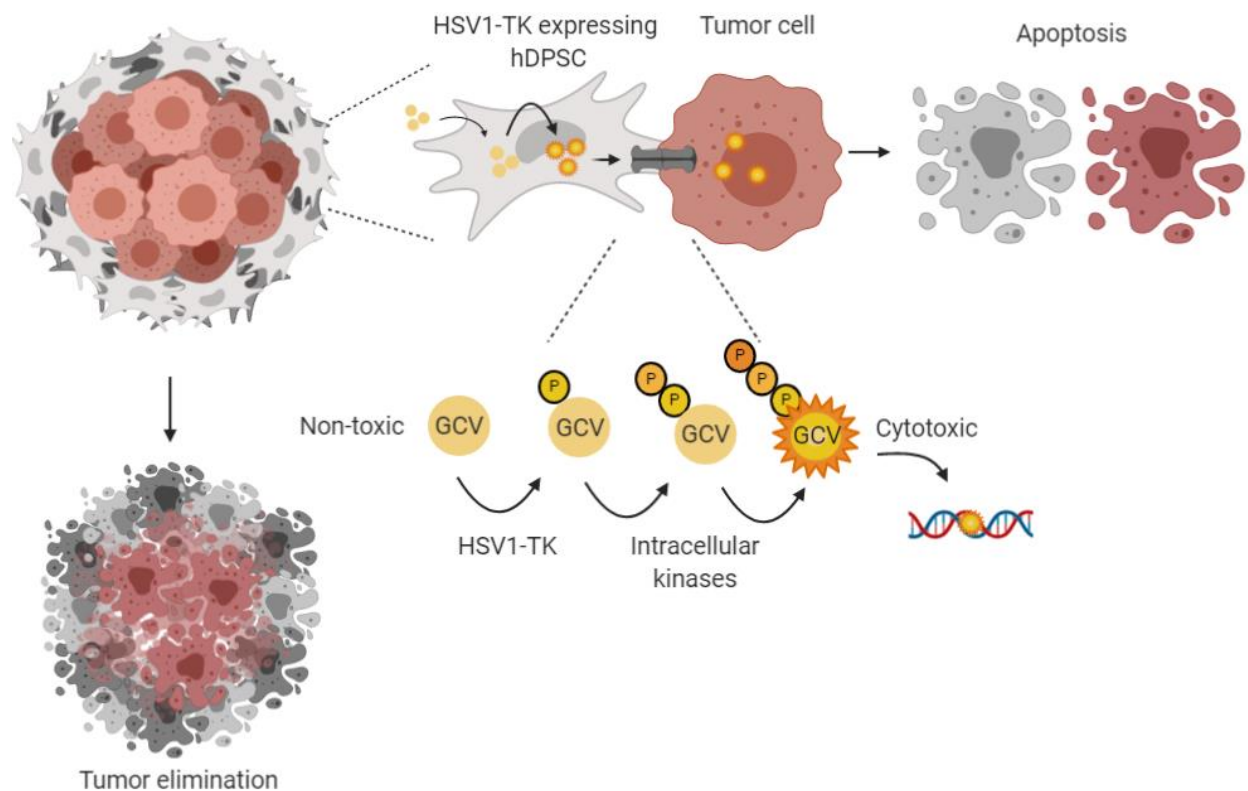

Fig. 1| An overview of the proposed mechanism of a stem cell-based suicide gene therapy for oral squamous cell carcinoma (OSCC). First, DPSC expressing the suicide gene Herpes Simplex Virus 1-thymidine kinase (HSV1-TK) must be obtained. These stem cells will then be administered, after which they should migrate towards the tumor site. Here, the dental pulp stem cells (DPSC) are expected to form communication channels with the tumor cells. Via those established channels, also referred to as gap junctions, substances smaller than 1000 Da can be exchanged through active diffusion. Subsequently, the prodrug ganciclovir (GCV) will be administered, and upon entry of an HSV1-TK-expressing stem cell, GCV should be phosphorylated by HSV1-TK to GCV monophosphate (GCV-P). Subsequently, further phosphorylation to its cytotoxic metabolite GCV triphosphate (GCV-3P) is conducted by intracellular kinases. The GCV-3P variant will disrupt the DNA synthesis process, eventually causing apoptosis of the affected cell. However, the cytotoxic substance must also be transferred to the neighboring cells via gap junctions formed between the DPSC and OSCC cells in order to be able to extend its toxic effect to the surrounding area, which then will possibly result in the elimination of the entire tumor while minimizing the adverse effect on the healthy tissue. *Figure made with BioRender*

potency for this application. However, their migration towards the tumor site has already been observed and validated *in vitro* by previous research of our group (data not shown). In this study, DPSC will be evaluated based on (1) their gap junctional communication capacity with cancer cells and (2) their ability to carry the suicide gene and their ability to convert GCV into its cytotoxic variant. The therapeutic effect of the HSV1-TK-transduced DPSC extensively relies on a locally provoked bystander effect in which the lethal drug spreads to the neighboring tumor cells. For this reason, a DPSC-OSCC co-culture system will be generated to evaluate the use of this stem cell type and the therapy *in vitro*. Preliminary data suggest that gap junctions are present and potentially responsible for the communication between these two cell types (data not shown). Therefore, gap junction intercellular contact is believed to establish the bystander mechanism in this setting, resulting in the cell death of both the tumor cells and DPSC. Hence, we hypothesize that GJIC between DPSC and OSCC cells will cause apoptosis of OSCC cells *in vitro* using the HSV1-TK/GCV system. Consequently, the main goal of this research is to determine the occurrence of gap junction formation and communication between DPSC and tumor cells. Furthermore, we will engineer and assess an HSV1-TK construct to generate suicide gene-expressing DPSC and test their potency in this therapy. Moreover, with this study, we aim to provide more insights into the use of DPSC as a vehicle in OSCC suicide gene therapy. This might resolve the therapy's major drawback currently in clinical settings involving the safety profile of the gene delivery systems.

EXPERIMENTAL PROCEDURES

Cell isolation and culture – Human dental pulp tissue was extracted from third molars collected after orthodontic surgery performed in Ziekenhuis Oost-Limburg (ZOL, Genk, Belgium). Each patient, or their guardian in case of minors, granted informed consent. DPSC were isolated from the human dental pulp tissue via the explant or outgrowth method described by *Hilkens P. et al.* (39). Afterwards, these DPSC were cultured in alfa-Minimum Essential Medium (α-MEM, M4526, Sigma-Aldrich, Belgium) supplemented with 1% penicillin-streptomycin (P/S, P4333, Sigma-

Aldrich), 2 mM L-glutamine (G7513, Sigma-Aldrich), and 10% heat-inactivated fetal calf serum (S1520, HI-FCS, Biowest) at 37°C, 5% CO_2 in a humidified area. After reaching passage ten, these cells were no longer used in any experimental procedure of this study.

The University of Michigan squamous cell carcinoma 14C (UM-SCC-14C) purchased from CLS Cell Lines Service (CVCL_7721, Germany) was cultured in Dulbecco's modified eagle medium F12 HAM (DMEMF12, Gibco, Ireland) enriched with 2 mM L-glutamine, 1% P/S, and 5% HI-FCS at 37°C, 5% CO_2 in a humidified area.

A DPSC-OSCC co-culture system was generated by seeding the DPSC and OSCC cells in a 1:1 ratio at 70-80% confluency (approximately $1,5 \times 10^4$ cells/cm²). These co-culture systems were cultured in the OSCC growth medium until 100% confluence was attained. Experimental procedures were conducted 48h after reaching the 100% confluence to ensure gap junction formation between the cells.

The Human Embryonic Kidney cell line 293T obtained (HEK293T, 85120602) from Sigma-Aldrich was cultured in DMEM (Gibco, Ireland) supplemented with 2 mM L-glutamine, 1% P/S, and 5% HI-FCS at 37°C, 5% CO_2 in a humidified area. Plates were coated with Poly-L-Lysine (PLL, 100µg/mL, Sigma-Aldrich) prior to cell seeding.

Plasmid construction – The first step to establish HSV1-TK-expressing DPSC involves the assembly of the HSV1-TK construct. An insert of variant 39 of the *HSV1-TK* gene (HSV1-sr39TK, Gambhir et al.) was cloned into an in-house generated pSin vector, resulting in the construct shown in **Suppl. Fig. 1A**. A control construct (**Suppl. Fig. 1B**) containing the reporter gene enhanced Green Fluorescent Protein (eGFP) was also produced through a similar process. Both inserts were purchased from Invitrogen. First, a restriction digest of the insert and empty vector pSin was conducted using MssI and EcoRI (**Suppl. Table 2**) to create equal cleaving ends on each component. Next, the samples showing the expected band pattern (GFP: ~ 2500 bp, HSV1-TK: ~ 3000 bp, pSin: ~ 7500 bp) were selected and purified using the Gel Clean-up Kit (Macherey-Nagel, Belgium). Subsequently, the obtained products were ligated using T4 DNA Ligase Kit (Thermo Fisher Scientific) together with the

considering T4 Buffer (1h, 22°C; 10 min, 65°C). Next, the ligation products were amplified by 5-alpha Competent *Escherichia (E.) coli* bacteria (C2987H, NEB, Belgium) and purified using the NucleoSpin plasmid (Macherey-Nagel) following the manufacturer's manual. Afterwards, the generated constructs were amplified by the 5-α Competent *E. coli* bacteria according to the manufacturer's guidelines and purified via the Nucleobond Xtra Midi EF kit (MN 740588, Macherey-Nagel). The NanoDrop^{TM} 2000 (Thermo Fisher) was used to evaluate the obtained samples' purity and concentration. A restriction digest (37°C, 30 min) was conducted using the appropriate restriction enzyme pairs, BcuI/MreI and NdeI/XbaI (**Suppl. Table 2**), to acquire the first indication whether the construct was produced correctly. Thereafter, HEK293T cells, and later DPSC, were transfected with Lipofectamine® 2000 Reagent (Invitrogen) according to the manufacturer's instructions.

Lentiviral vector construction, production, and DPSC transduction – DPSC were transduced by a second-generation lentiviral vector system. HEK293T cells were used to produce the lentiviral particles as described by Tiscornia et al. (42). For DPSC transduction, the cells were seeded at 2,5 x 10^3 cells/cm² in a 24-well plate. The following day, the obtained lentiviral particles were added to the cultured DPSC in a dilution series (10, 20, 30, 60 µL/well). Selection of transduced DPSC was based on their puromycin resistance. Therefore after 7 days, the cells were treated with puromycin (1 µg/ml, #ant-pr-1, InvivoGen, France) every 3 days.

Immunocytochemistry staining (ICC) – 3,3'-Diaminobenzidine (DAB)/Horseradish peroxidase (HRP) and immunofluorescent (IF) stainings were performed to analyze the expression of various markers of which a detailed overview is provided in **Suppl. Table 3**. For all experiments, the cells were seeded on glass coverslips and fixed with Unifix (VWRK4031-9010, Klinipath, Belgium) for 20 min, followed by cell permeabilization with 0.05% Triton (X100, Sigma-Aldrich) in 1x Phosphate buffered saline (PBS) for 15 min at 4°C when required (intracellular marker). Next, the cells were incubated in a 10% serum-free protein block (K4061, Dako, Belgium) for 1h at room temperature (RT) to prevent unspecific antibody binding. Subsequently, the appropriate primary antibody (**Suppl. Table 3**) was incubated overnight at 4°C. The next day, different steps were conducted to complete the DAB- and IF-staining: *DAB* – The Envision Dual Link System-HRP kit (K4061, Dako) was used as a secondary reagent and incubated for 30 min. Subsequently, the cells were incubated with Liquid DAB$^+$ Substrate Chromogen System (K3468, Dako) for a maximum of 8 min, followed by a counterstaining with Meyer's Hematoxylin. The coverslips were washed with tap water and mounted with the aqueous-based Immu-Mount solution (9990402, Thermo Fisher). Images were acquired using the Leica DM 2000 Light Microscope. *IF* – The appropriate fluorescent secondary antibody (**Suppl. Table 4**) was incubated for 1h, following a 10 min nuclear staining with 4',6-diamidino-2-phenylindole (DAPI; #D9542, Sigma-Aldrich) both performed in the dark. The coverslips were also mounted with Immu-Mount (Thermo Fisher). The results were visualized with the DM 4000 Fluorescent Microscope (Leica) and analyzed via ImageJ software.

Functional analysis of the gap junctions – The gap junction functionality was assessed via a Lucifer Yellow dye transfer assay. DPSC were seeded in a 35 mm dish with a glass bottom (MatTek corp). For the co-culture experiments, DPSC and UM-SCC-14C cells were seeded in a 1:1 ratio. Both conditions were cultured until a 100% confluency was achieved. After an additional two days, one single cell was microinjected with the Lucifer Yellow dye (428/536 nm, L0144, Sigma-Aldrich) while simultaneously visualized underneath the ELYRA super-resolution microscope (ZEISS). Every other 30s a snapshot was taken that were merged into a short film afterward using the ZEN blue software (ZEISS).

Optimization of the co-culture multicolor staining – Several conditions were examined to visualize the DPSC and OSCC cells simultaneously in live and fixed cultures. Following dyes were applied according to the manufacturer's instructions before co-culturing the cells as described before: Cell Mask Deep Red (CMR, 1: 1000, C10046, Thermo Fisher), Fast 1,1'-Dioctadecyl-3,3,3',3'-Tetramethylindocarbocyanine Perchlorate (DiI, 1:1000, D3899, Thermo

Fisher), ViaFluor® SE 405 (1:1000, 30068, Biotium) and 488 (1:4000, 30086, Biotium). An ICC-based live-staining was performed by 30 min incubation of both the primary and secondary antibody diluted in sterile PBS at 37°C each. The cells were imaged using the DM 4000 Fluorescent Microscope (Leica), LSM 880 confocal microscope (ZEISS), and Axiocam 208 Color (ZEISS).

One-Glo^{TM} Luciferase Assay – DPSC were seeded in duplo with a 1,25 x 10^3 cells/cm² density in a 24-well plate (Greiner Bio-One Cellstar) and transfected with the HSV1-TK or eGFP construct 48h later, followed by an additional incubation of 72h. The Fluc activity was measured via the One-Glo^{TM} Luciferase Assay System (Promega) according to the manufacturer's instructions and analyzed with Bioluminescence Imaging (BLI, IVIS Lumina III, Perkin Elmer). GFP-FLuc-expressing DPSC (provided by Prof. dr. Annelies Broncaers) were used as a positive control, while non-transfected DPSC served as a negative control group.

In vitro GCV administration– In the first phase, a pilot experiment was conducted on HEK293T cells to evaluate the HSV1-TK construct's function. Cells were seeded at 2,5 x10^3 cells/cm² and transfected two days later with Lipofectamine® 2000 Reagent (Invitrogen) according to the company's protocol. 48h later, several concentrations of GCV (1µM, 10 µM, 100µM; Cymevene®, CheplaPharm, Belgium) diluted in growth medium were administered to the cells. The next day, GCV was added for a second time to the cells. The effect of GCV was monitored by the number of dead cells in each condition and imaged using the Axiocam 208 Color (ZEISS) the day after each treatment. Afterward, this experiment was repeated in a DPSC monoculture following the same protocol.

Statistical analysis – No statistical analyses were performed due to absence of quantitative data.

RESULTS
In this project, we aimed (1) to validate GJIC between DPSC and OSCC cells *in vitro* and (2) to generate the HSV1-TK and eGFP control construct (3) in order to eventually establish and evaluate the potency of HSV1-TK-expressing DPSC in suicide

gene therapy. Therefore, gap junction formation between the DPSC and OSCC cells was characterized via connexin-43 immunostaining first. Next, the GJIC will be functionally analyzed via a Lucifer Yellow dye transfer assay to ensure the gap junctions' role as the primary mechanism of action causing the bystander effect. Furthermore, the experimental and control construct were engineered to generate HSV1-TK- and eGFP-expressing DPSC. Thereafter, these cells were evaluated, and a pilot experiment was conducted to provide a basis of the GCVs cytotoxicity *in vitro*.

Gap junctional communication between DPSC and OSCC
Cx43 *expression is observed in an in vitro DPSC-OSCC co-culture model* – Gap junctional communication between stem cells and tumor cells is a crucial factor in our proposed stem cell-based suicide gene therapy. Therefore, a co-culture model was established to investigate the role of gap junction formation and communication between those cells *in vitro*. DPSC and OSCC cells can be distinguished based on their morphology using light microscopy (LM). More specifically, DPSC (blue arrow, **Fig. 2B**) have a spindle-shaped and a stellate morphology, while OSCC cells (orange arrow, **Fig. 2B**) have a rather round shape. Moreover, DPSC are larger in size compared to the tumor cells (**Fig. 2A, 2B**). Additionally, a DAB ICC staining was performed with a cell-specific marker inherent for each cell type. CD105 was used to visualize the DPSC and Cytokeratin (Ck) to indicate the tumor cells shown in **Fig. 2C** and **Fig. 2D**, respectively (n=3). A dark brown signal was observed for each marker in the correct cell type demonstrating the possibility to stain both cell types separately in our co-culture model, which is crucial for future experiments.

Moreover, the presence of connexin 43 can be the first indication of gap junction formation between cells. Therefore, an immunofluorescence staining was performed and indicated Cx43 expression in both DPSC (**Fig. 3A**) and OSCC (**Fig. 3B**) cultures separately, as well as in the co-culture model (**Fig. 3C** and **3D**) (n=3). Moreover, the expression of Cx43 on the cell surface appeared to be higher in more cell-dense areas. **Fig. 3D** shows a more detailed image (100x magnification) of the co-culture. The expression of Cx43 is precisely
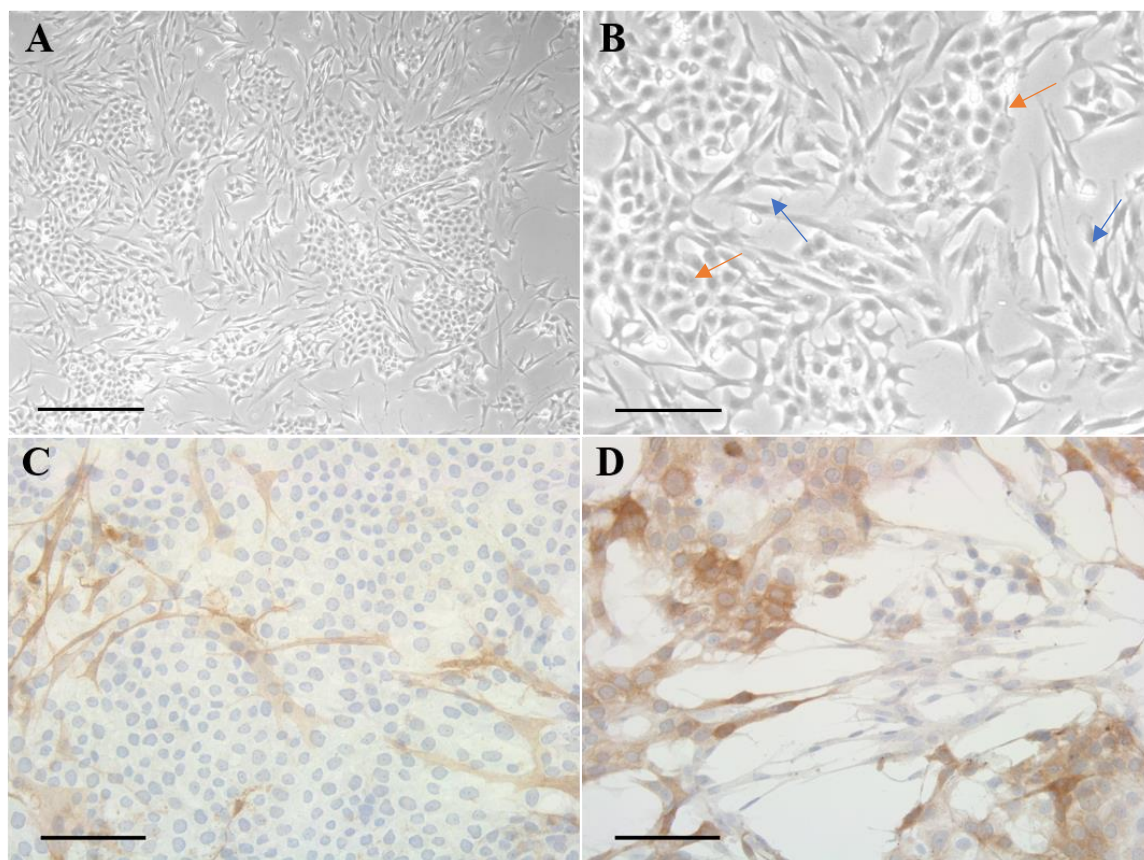
Fig. 2| The co-culture model composed of dental pulp stem cells (DPSC) and the oral squamous cell carcinoma (OSCC) cell line. The DPSC and OSCC were seeded in a 1:1 ratio and cultured in DMEM/F12 supplemented with 2.5% Fetal Calf Serum, 2 mM L-glutamine, and 1% penicillin/streptomycin. **(A)** The OSCC cell groups were surrounded by DPSC in the co-culture model. **(B)** The DPSC (blue arrow) and OSCC cells (orange arrow) can be morphologically distinguished by their spindle- and more circular-shaped form, respectively. Additionally, a diaminobenzidine (DAB)-based immunochemistry staining using cell-specific markers was performed to validate the presence of **(C)** DPSC via CD105 and **(D)** OSCC cells through cytokeratin (Ck). All images were obtained via light microscopic analysis using the DM2000 Led light microscope (Leica). N=3. Scalebar **(A)** 200 µm, **(B-D)** 100 µm. Magnification: **(A)** 10x, **(B-D)** 20x.

demonstrated at the plasma membrane of adjacent cells by small spots with a more intense fluorescent signal (yellow arrow, **Fig. 3D**). This might indicate cell-cell contact at this location. Similar observations can be made in de DPSC- and OSCC-cultures separately, as seen in **Fig. 3A** and **3D**, respectively.

Preliminary data suggest gap junctional intercellular communication in the in vitro study model – The indication of gap junction formation via Cx43 alone is not enough to validate their role in our proposed therapy. Therefore, it is important to also monitor their functional activity. Hence, a Lucifer Yellow dye transfer assay was performed in a DPSC culture (**Fig. 4A**) and in co-culture with

OSCC (**Fig. 4B**). During this assay, the transfer of Lucifer Yellow was observed from the patched cell to its neighboring cells in real-time. In **Fig. 4**, representative images of the obtained data are shown with an overview of the dye transfer throughout the cultures in time. In both the DPSC culture and co-culture model, transfer of Lucifer yellow from the injected cell to adjacent cells was observed through spreading of the dye in a several minutes time range. This indicated that gap junctional intercellular communication occurred in our *in vitro* model.
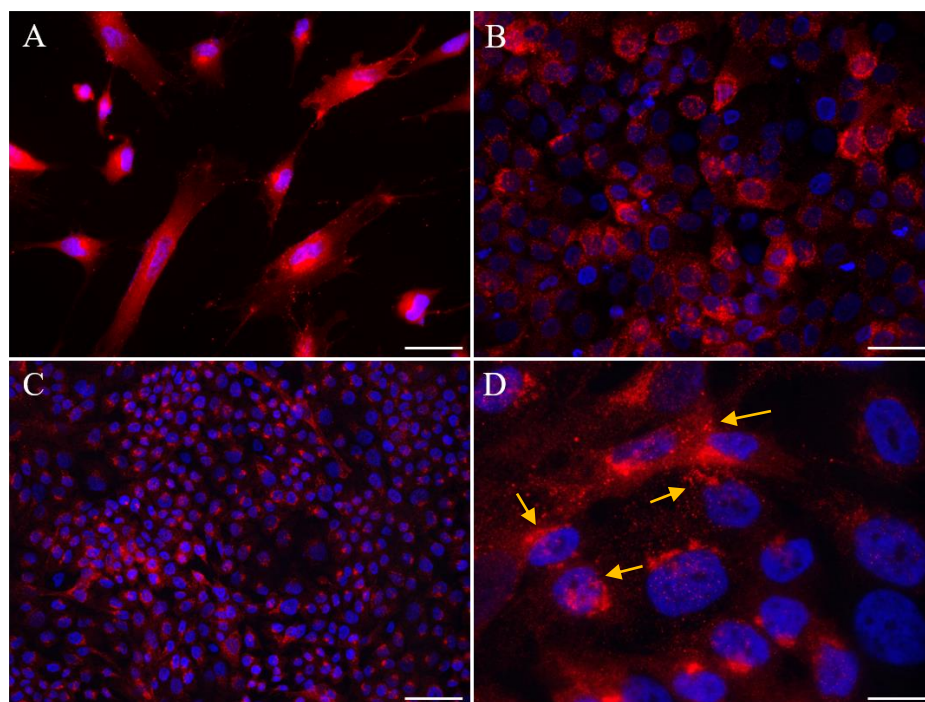
Fig. 3| Connexin 43 expression is demonstrated in the co-culture model, indicating the presence of gap junctions between DPSC and OSCC. Representative fluorescent images of connexin 43 (Cx43) expression in DPSC **(A)** and OSCC **(B)** monocultures and the co-culture model **(C, D)**. The DPSC and OSCC were seeded separately **(A, B)** and in a 1:1 ratio at 1.5×10^4 cells/cm² and cultured in the proper growth medium until a confluence of 100% was reached, after which another two days passed before the start of any experiment to assure gap junction formation. Afterward, Cx43 expression in the cultures was evaluated by immunofluorescence. In each of the cultures, Cx43 was expressed by both cell types throughout the whole culture. **(D)** Higher Cx43 expression indicated by a more intense fluorescent signal was observed in more cell dense region and in the borders of two adjacent cells (yellow arrow). Images were obtained by the DM 4000 Fluorescent Microscope (Leica). N = 3. Scalebar = **(A-C)** 75 µm, **(D)** 10 µm . Magnification **(A, B)** 20x, **(C)** 10x, **(D)** 100x.
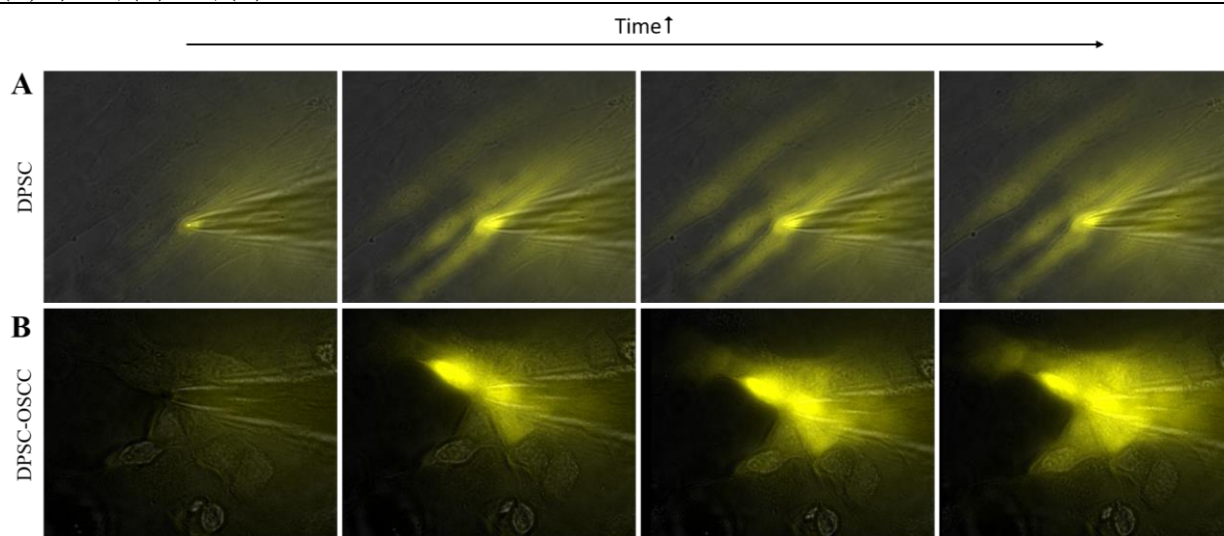

Fig. 4| Functionally active gap junctions are present in the co-culture system. Cells were seeded and cultured until a 100% confluency was reached. Then another two days passed to allow gap junction formation between the cells prior to assessing their functionality via the Lucifer Yellow dye transfer assay. Therefore, one single cell was micro-injected with Lucifer Yellow (428/536 nm), and a time series of snapshots were taken every 30 s by the ELYRA super-resolution microscope. Representative images of this functionality assay in a DPSC **(A)** and co-culture **(B)** are shown and demonstrate the transfer of the dye to adjacent cells in both cultures over time. Magnification 63x

Visualization of stem and tumor cells simultaneously in the in vitro study model – Thus far, we showed that connexin 43 is expressed throughout the co-culture in more cell-dense regions. The indication for a dense region was based on the higher number of nuclei counterstained with DAPI in those specific areas. However, no clear distinction could be made between the OSCC cells and DPSC in the fluorescence microscopic images. For this study, it is crucial to validate the gap junction formation and communication between both stem cells and tumor cells. Therefore, we aimed to visualize both cell types individually so that a better distinction between the DPSC and OSCC cells could be made when studying the cell-cell interactions in both fixed and live-cell cultures. **Fig. 5** demonstrates an overview of the best outcome conditions of our optimization process.

In the first condition, shown in **Fig. 5A**, a combination of a membrane dye and stem cell marker was used. Here, the tumor cells were stained with CMR, and the DPSC, on the other hand, were visualized with CD105/Alexa Fluor 555. The fluorescent signal of the latter was quite specific for the DPSC only. However, the CMR dye used to visualize the OSCC cells also appeared to have spread to the DPSC in the culturing process, resulting in non-specific signal throughout the whole culture. Although the overlay image of this condition was acceptable, we aimed to gain higher specificity and less background. Therefore, a similar experiment was performed. Here the OSCC cells were stained with Fast DiI, and the DPSC were visualized with CD105/Alexa Fluor 488 to avoid fluorescent overlap (**Fig. 5B**). Again, in this condition, the membrane dye DiI seemed to have dispersed to the DPSCs causing a non-specific signal. However, the composite image showed a reasonable presentation of each cell type in the co-culture model.

Additionally, a live cell staining experiment was conducted on the co-culture model using CD105 in combination with the secondary antibody Alexa 488. No pronounced expression of CD105 was observed in the cultures compared to the background signal. Moreover, the DPSC showed an aberrant morphology. The cells were less stretched and they were detaching from the surface.

Additionally, dying cells were also noticed to some extent as well (data not shown).

In the last condition, ViaFluor® 405 and 488 were used to stain the DPSC and OSCC cells, respectively (**Fig. 5C**). Here, almost no background or non-specific signal was observed for both cell types resulting in a refined overview of the DPSC and tumor cells during live-imaging of the co-culture. Moreover, all the cells appeared healthy with a normal morphology. Nevertheless, few remainders of both dyes seem to be noticed in this condition. This can possibly be avoided by an additional washing step before imaging. Equal results were obtained in fixed cultures (data not shown). In summary, the highest quality staining was obtained by staining the cells with the ViaFluor® SE Proliferation Kit and will be used in future experiments to visualize the DPSC and OSCC cells simultaneously.

Successfully engineered experimental and control construct

In order to establish HSV1-TK- and eGFP-expressing DPSC, the constructs were generated. The final products of the cloning process are shown in **Suppl. Fig. 1**. Each construct contained a human elongation factor-1 alpha (EF1a) promoter to drive the gene expression and was designed to express HSV1-TK **(Suppl. Fig. 1A),** or eGFP **(Suppl. Fig. 1B)** linked to a Flag- and His-tagged Firefly Luciferase (FLuc) and puromycin resistance cassette via a peptide2A (T2A) sequence and internal ribosome entry site (IRES), respectively. Additionally, ampicillin resistance (AmpR) was also included in each transfer plasmid. To obtain a first indication whether the construct clones were ligated correctly, a restriction pattern was generated using the restriction enzyme pairs XbaI/NdeI and BcuI/MreI. The expected band pattern was observed for five replicates of the HSV1-TK construct and six replicates of the control construct (data not shown).

In vitro **confirmation of the transfection and functionality of the experimental and control construct**

After engineering the constructs, a pilot experiment involving the transfection of the HEK293T cell line was performed. Here, we aimed to assess the function of the HSV1-TK-Fluc-Flag-His and eGFP-Fluc-Flag-His constructs.
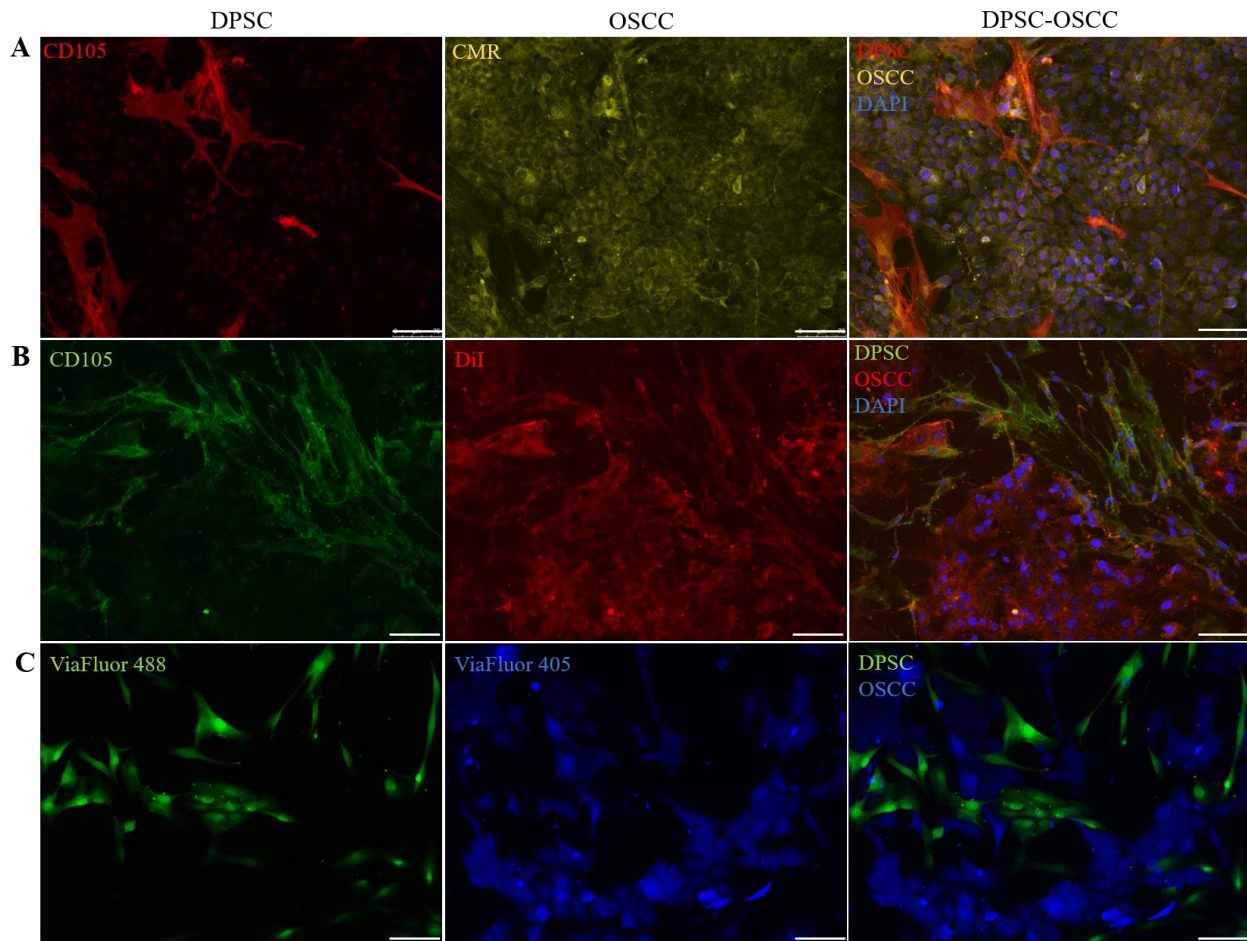
Fig. 5| Optimization of a co-culture multicolor staining. Several conditions were tested to visualize the dental pulp stem cells (DPSC) and oral squamous cell carcinoma (OSCC) cells separately to emphasize the cell-cell interactions between the two cell types specifically. The DPSC and OSCC were seeded in a 1:1 ratio at 1.5×10^4 cells/cm² and cultured in DMEM/F12 supplemented with 2.5% fetal calf serum (FCS), 2 mM L-glutamine, and 1% penicillin/streptomycin until a confluence of 100% was reached. The OSCC were stained with membrane dyes **(A)** Cell Mask Red (CMR) or **(B)** 1,1'-Dioctadecyl-3,3,3',3'-Tetramethylindocarbocyanine Perchlorate (DiI) prior to being (co-)cultured, while the DPSC were visualized via immunofluorescence with CD105 in combination with **(A)** Alexa Fluor 555 and **(B)** Alexa Fluor 488 after fixation. **(C)** The last condition involves visualization of cell types with the proliferative dye ViaFluor 405 (DPSC) and ViaFluor 488 (OSCC). **(A, B)** When combining the membrane dyes with antigen labeling through immunocytochemistry, non-specific signal was noticed in both conditions. The overlay images showed a reasonable overview of the co-culture model in which the DPSC could be adequately identified from the OSCC cells. **(C)** In the last condition, the least background as well as the highest specificity was observed for both cell types resulting in a refined overview of the DPSC and tumor cells in a co-culture. Moreover, this staining protocol showed the most ideal results for both experiments since life-labeling of the DPSC was failed. Images of **(A, B)** were obtained using the DM 4000 Fluorescent Microscope (Leica). Images of **(C)** were acquired with the LSM 880 confocal microscope (ZEISS). Scalebar =75 µm. Magnification 20x.

As demonstrated in the representative ICC images, both the eGFP- and HSV1-TK-transfected cell populations stained positive for each marker – GFP, Flag-, and His-tag (**Fig. 6.A**) – and – HSV1-TK, Flag-, and His-tag (**Fig. 6.B**) –, respectively. Furthermore, no expression of the markers was observed in the non-transfected control groups. Also in the conditions omitting the primary antibody, no signal was detected, implying that there was no aspecific binding of the secondary antibody. With these results, a first step towards the confirmation of the constructs in HEK293T cell culture was made.

Next, the functionality of the HSV1-TK gene was examined via GCV administration to HSV1-TK-expressing HEK293T cells. **Fig. 6.C** provides

an overview of representative images obtained at the endpoint of this experiment. Here, a decrease in cell density was visually observed after administration of GCV compared to all control groups. The culture confluencies are estimated at 95%, 70%, 50%, and 30% for 0 µM, 1 µM, 10 µM, and 100 µM, respectively. More specifically, lower cell densities were observed with administration of higher GCV dosages. Moreover, detached and floating cells were observed in the medium of the cells exposed to any concentration of GCV

experimental conditions. Furthermore, repeated (2 doses) and prolonged exposure (4 days) to GCV appeared to attribute to more cell death. In contrast, all cells were still attached and appeared to have a normal morphology when GCV was administrated without the presence of HSV1-TK (+ GCV - HSV1-TK) or after transfection (-GCV + HSV1-TK) itself. Taken together these findings, further verification of an expressed and functional HSV1-TK suicide gene was obtained in a dose- and time-dependent manner.
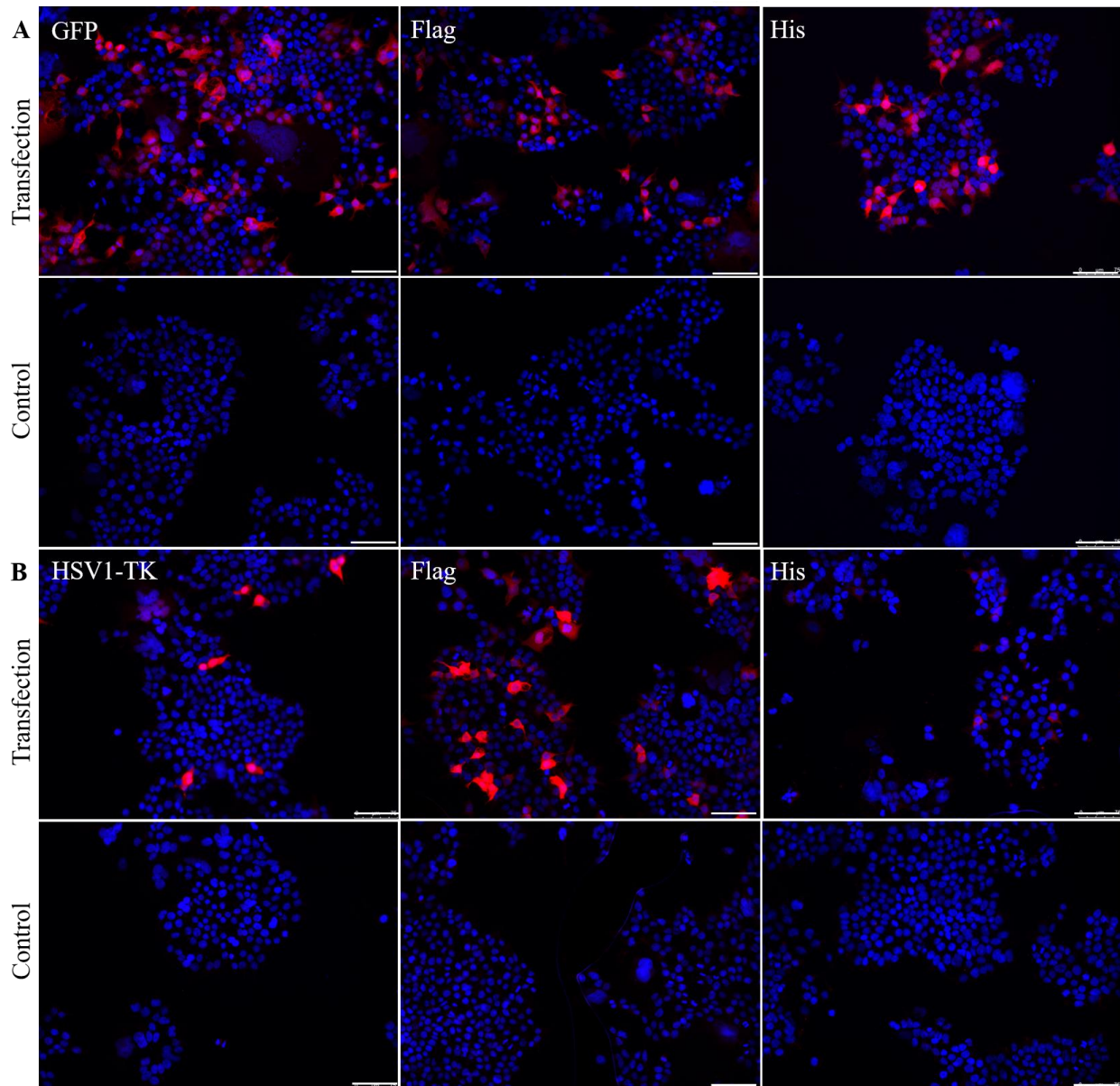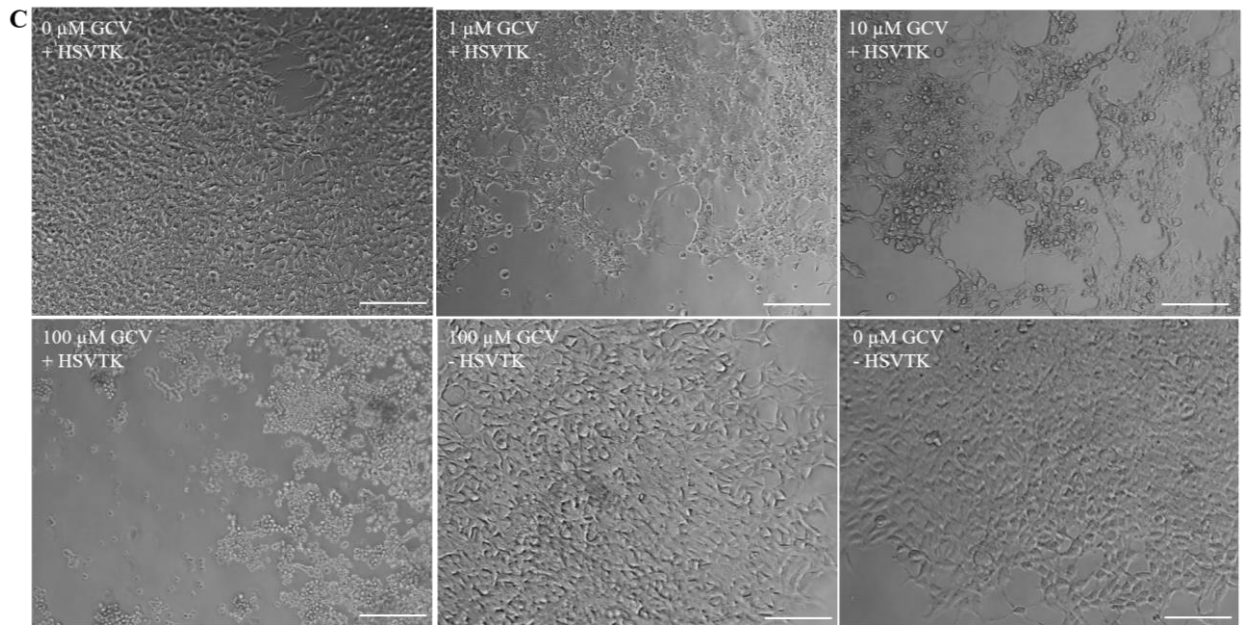

*Fig. 6

Fig. 6| Generation of eGFP- and HSV1-TK expressing HEK293T. A pilot experiment was conducted to evaluate the presence of **(A)** the control and **(B)** experimental construct in transfected HEK293T cells. Cells were seeded at $2,5 \times 10^3$ cells/cm² and transfected two days later. The next day, an immunofluorescent analysis was performed to assess GFP, HSV1-TK, His- and Flag-tag expression in the transfected cells. For both constructs, expression of all markers was observed. No signal was present in the non-transfected control groups. Images were obtained using the DM 4000 Fluorescent Microscope (Leica). **(C)** Additionally, the functionality of the experimental plasmid was also assessed. Cells were seeded at 2×10^4 cells/cm² and transfected after 48h. Cells received ganciclovir treatment (1 µM, 10µM, 100µM) 48h and 72h after transfection. Final images were acquired after a three-day ganciclovir exposure by the Axiocam 208 Color (ZEISS). A could be observed with **(A, B)** N =2. **(C)** N= 3. Scalebar = **(A, B)** 75 µm, **(C)** 100 µm. Magnification **(A, B)** 20x, **(C)** 10x. *HSV1TK; Herpes Simplex Virus 1 thymidine kinase, eGFP; enhanced Green Fluorescent Protein, GCV; ganciclovir.*

A similar approach was applied to evaluate the constructs in DPSC. An additional test was conducted to validate the construct's functionality. The One Glo Luciferase assay confirmed Fluc expression in all replicates of both constructs (data not shown), suggesting their functionality. Furthermore, the function of the HSV1-TK gene was validated in DPSC after transfection. **Fig. 7.A** presents representative images of the (non-) transfected DPSC cultures after GCV exposure. The results obtained in this experiment are similar to those acquired in the HSV1-TK transfected HEK293T cells. Again, fewer cells are observed to be present in conditions with a higher GCV concentration as well as the control groups. No toxic effect of GCV exposure to non-transfected cells could be observed. In summary, these data suggest that GCV-induced cell death occurred in cells transfected with the suicide gene. Despite those promising findings, ICC images shown in **Fig. 7.B** demonstrated the lack of GFP and Flag-tag

expression in transfected DPSC, while an adequate signal was observed in eGFP-transduced DPSC, which were used as a positive control in this experiment. Again, no signal appeared to be present in the cell population.

DISCUSSION

OSCC is a growing health issue worldwide associated with increasing incidence and morbidity (43). Regardless of recent improvements in early detection and diagnosis of OSCC, current treatment strategies are still not sufficient enough to significantly ameliorate the 5-year survival of this disease (7, 44, 45). Hence, a more targeted treatment approach is desired to improve current treatment strategies. Suicide gene therapies employing the HSV1-TK/GCV system have shown promising results of anti-tumor control in a preclinical setting for various cancers (31, 46, 47).
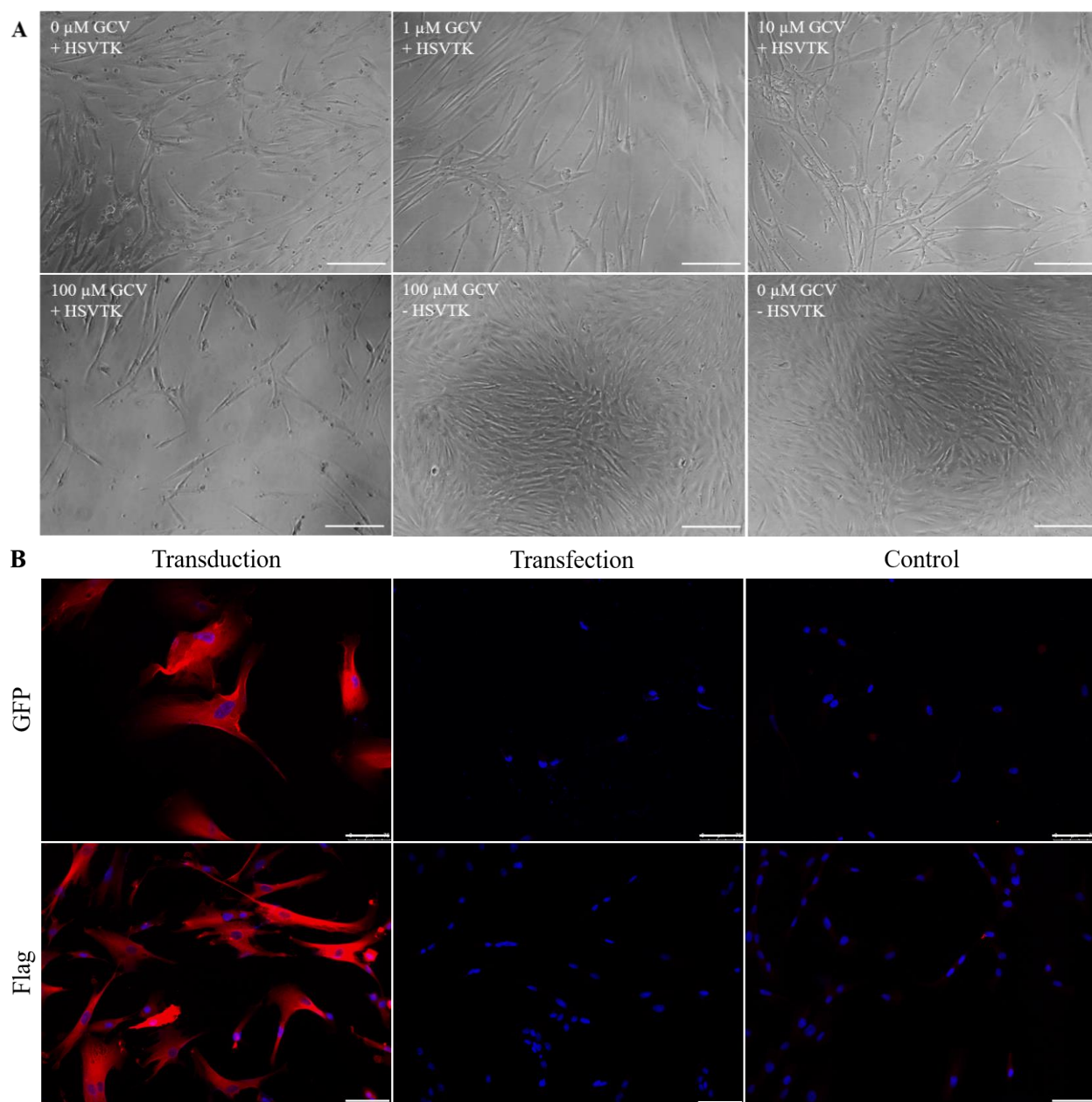
Fig. 7| Successful DPSC transfection was indicated by GCV-induced cell death, while contrary findings were observed via ICC. (A) Functional analysis the HSV1-TK gene was also assessed in DPSC. Cells were seeded at 2 x 10^4 cells/cm^2 and transfected after 48h. Cells received ganciclovir treatment (1 µM, 10µM, 100µM) 48h and 72h after transfection. Final images were acquired after a four-day ganciclovir exposure by the Axiocam 208 Color (ZEISS). A smaller cell population compared to the control groups was observed in each GCV condition, indicating the occurrence of cell death. Moreover, fewer cells are present in cultures treated with higher GCV dosages. **(B)** Immunofluorescent analysis against GFP and the Flag-tag was performed to evaluate the construct's functionality in DPSC. A positive (GFP-transduced DPSC) and negative (non-transfected DPSC) control were included. The expression of GFP and Flag was only observed in the GFP-transduced DPSC. Images were acquired using the DM 4000 Fluorescent Microscope (Leica) **(A)** N = 1. **(B)** N= 2. Scalebar = **(A)** 100 µm, **(B)** 75 µm. Magnification **(A)** 10x, **(B)** 20x. *HSV1TK; Herpes Simplex Virus 1 thymidine kinase, eGFP; enhanced Green Fluorescent Protein, GCV; ganciclovir.*

However, no desirable clinical significance is achieved until this moment due to safety and efficiency issues related to the viral gene delivery systems (11, 48). Therefore, in this study, the potency of DPSC as a vehicle of the suicide gene therapy will be evaluated to tackle this problem.

First, a co-culture system consisting of DPSC and OSCC cells was produced to function as the *in vitro* study model of this project. Besides morphological differentiation of these cells, a marker-based distinction was provided via ICC analysis. CD105, or endoglin, is a cell-surface marker classified by the ISTC MSC as one of the inherent surface makers of MSC along with CD73 and CD90. It is involved in the TGF-beta pathway and also abundantly expressed in vascular endothelial cells (49). OSCC cells were indicated by the expression of Ck using an antibody reactive against Ck 5, Ck6, Ck8, Ck17, and Ck19. Ck are the proteins composing the cytoskeleton of epithelial cells and are associated with various functions such as the cell's integrity, protection from mechanical and non-mechanical stress, and apoptosis (50, 51). Ck19 is known to have an increased expression in different cell types including, among others, OSCC, and non-sentinel lymph node (breast cancer) (52, 53). Moreover, Alix-Panabières et al. demonstrated the active release of Ck19 by tumor cells in the bone marrow and linked this process to metastatic progression of the tumor (51). Recently, it has been suggested by Rajeswari et al. as a biomarker for early detection of OSCC (52). In conclusion, we demonstrated the identification of DPSC and OSCC cells individually in the co-culture model, which implies the possibility.

Gap junction formation and intercellular communication between DPSC and tumor cells are vital in this proposed stem cell-mediated suicide gene strategy. In essence, our data showed cell-surface Cx43 expression in cell-dense regions of DPSC and OSCC cell-cultures individually as well as together in co-culture. Brockmeyer et al. also demonstrated Cx43 expression on the membrane of tumor cells, more specifically in tissue samples of OSCC patients (30). Furthermore, the group of Luzuriaga showed high expression of Cx43 in DPSC cultures (54). Although Cx43 expression is an indicative factor for the presence of gap junction channels, it is no solid evidence ensuring gap junction formation or functionality between adjacent cells. As described before, clustering of six connexin units produces a hemichannel that, when connected to another hemichannel, will give rise to the formation of a gap junction between adjacent cells (29). Therefore, to strengthen these first results, a functionality assay involving the micro-injection of Lucifer yellow was performed. The outcome of this experiment indicated the transfer of the fluorescent dye from the injected cell to its neighboring ones in a DPSC- and co-culture model over time, further supporting the evidence of GJIC between stem and OSCC cells. Another commonly used method to assess GJIC, which requires less specialized material or skilled personnel, is the scrape loading-dye transfer assay. Here, Lucifer Yellow is introduced into the cell by creating a clean cut resulting in absorption of the dye by the injured cells from which the transfer to adjacent cells will be observed (55-57). Miletic et al. employed another principle to illustrate the GJIC between bone marrow-derived MSCs and glioma cells. Instead of using Lucifer Yellow, calcein-AM was used as non-membrane-permeable dye that can transfer to other cells in the culture via gap junctions. In this experimental setup, one cell type was stained with the membrane dye DiI and the other cell population was labeled with calcein-AM before brought together in co-culture. Upon incubation, gap junctional transfer of calcein-AM can occur if GJIC is possible. The presence of GJIC can be analyzed by flow cytometry (31).

To this point, discrimination between different cell types in the co-culture model was based solely on the cell's morphology when investigating GJIC. Therefore, we aimed to optimize a multicolor staining to both distinguish GJIC between tumor and stem cells. Three different staining methods were tested and evaluated. The two first approaches involved the usage of a membrane dye combined with immunofluorescent visualization of the stem cell marker CD105. Both DiI and CMR are substances with an amphipathic character allowing their integration into the plasma membrane. According to the manufacturer's guidelines, the staining of the membrane with CMR is more uniform than DiI. Ragnarson et al. illustrated DiI's compatibility to pre-label cells in co-culture over a more extended period (one week), which has not been evaluated for CMR yet (58, 59). Despite these findings, an aspecific signal was

observed for both dyes when staining the tumor cells in the co-culture model. We presumed that due to long-term culturing, which is required for gap junction formation, both dyes would internalize because of membrane turnover eventually (60). This is followed by the excretion of the dye through apoptotic bodies (31). Subsequently, those vesicles can be included in neighboring cells through endocytosis, causing minor cross-staining of the DPSC (55). However, the fluorescent signal of the DPSC marker itself was more robust, exceeding this background signal. In the last condition, the proliferative dye ViaFluor SE® was employed to stain both cell types. This dye has another mechanism of action. Upon entry of the cell, the dye is hydrolyzed by endogenous esterases that activate the fluorescent compound of the dye, which then interacts with intercellular proteins to establish a stable fluorescent signal preserved in that cell only. Moreover, ViaFluor® is passed on during proliferation, making it an ideal candidate for our live and fixed co-culture experiments. In those experiments, the stained cells have to be in culture for a prolonged time to ensure gap junction channel formation, making this the most refined multicolor staining condition (61). As described earlier in the DiI/calcein-AM assay, a discrimination between the two cell types of the co-culture was also made through prior labeling of one cell population with a membrane dye, while the other was visualized with the transfer dye itself (31).

In summary, our results suggested the occurrence of GJIC between stem cells and tumor cells in the co-culture model. However, these data can be reinforced by employing the optimized multicolor staining settings to emphasize the connection between the DPSC and OSCC cells since this is one of the crucial factors in the therapy's principle. Therefore, it would be relevant to evaluate the Cx43 expression and functional activity of the gap junctions again in these settings.

Furthermore, in order to generate HSV1-TK-expressing DPSC, an EF1a-HSV1TK-T2A-Fluc-Flag-IRES-PuroR-AmpR transfer plasmid was engineered first. The constitutive promoter EF1a was used to drive the gene expression. It has the ability to generate high levels of gene expression in a broad range of target cells, however awareness of its potency to cause transactivation is crucial (62).

Furthermore, the HSV1-sr39TK variant was used as suicide gene in this project. Black et al. demonstrated that this gene was able to hinder tumor growth by administration of a lower prodrug concentration. This GCV concentration did not evoke an effect in the cells expressing the non-mutant HSV1-TK for which a higher GCV dosage is required to achieve cell elimination. This offers a more effective alternative compared to the wild-type gene due to the higher catalytic function of the SR39 mutant (22, 63). On the other hand, the control construct expressed eGFP instead of HSV1-TK. eGFP is a widely known reporter gene. Moreover, eGFP can also be employed to visually observe a successful transfection/transduction due to its autofluorescent capacity (49, 64). Furthermore, a T2A sequence and IRES were also included in creating a polycistronic vector, meaning multiple genes can be expressed at the same time (65). The expression plasmid also included a FLuc domain which can be used as a confirmation tool of successful transduction and future-oriented it can be applied as a stem cell tracker for in vivo follow-up of DPSC migration and tumor homing, both analyzed with BLI (64). Finally, two resistance cassettes were included in each vector. The ampicillin resistance is of use in the amplification steps of the construct by the 5-alpha Competent *Escherichia (E.) coli* bacteria as a selection marker. Furthermore, transduced DPSC were selected based on the presence of a puromycin resistance cassette, thereby creating an homogenous pool of GFP- or HSV1-TK-expressing DPSC. Both constructs will be sequenced to verify the sequence of the constructs and the absence of mutation.

To acquire a first indication of the construct's functionality, HEK293T cells were transfected with the HSV1-TK construct. First, it was confirmed by the expression of HSV1-TK, GFP, Flag-, and His-tag in part of the transfected cells after immunofluorescent analysis. The partial marker expression in the transfected HEK293T cultures can be due to an inefficient transfection resulting in only a small number of transfected cells. Additionally, GCV was administered to transfected HEK293T cultures to evaluate the HSV1-TK gene's function in a stable cell line. In this experiment, cell death was observed in all conditions in a dose-depend manner, suggesting a properly functioning construct. Moreover, no

decrease in cell density was detected in any of the control groups, implying that GCV or the transfection protocol did not influence the results of this experiment. A similar effect of the HSV1TK/GCV system was demonstrated by Li et al. and Militec et al. in the context of glioma therapy (31, 63). Next, the same procedures were performed on DPSC cultures. Here, BLI confirmed the presence of the HSV1-TK and eGFP plasmids by bioluminescence emission for each replicate. Additionally, a decrease in cell density was observed after GCV administration, suggesting a properly functioning suicide gene. However, this was not confirmed via ICC for both constructs due to the lack of expression of any of the construct markers. Therefore, additional ICC analysis of the control construct was conducted. Here, eGFP-transduced DPSC were included as a positive control to evaluate the GFP and Flag antibody specificity and functionality. Also, no fluorescent signal was obtained in ICC against GFP in eGFP-transfected DPSC, while an adequate signal was observed in the positive control group. Despite these unsuccessful findings concerning ICC in transfected DPSC, this will have no major impact on further research. HSV1-TK- and eGFP-transfected DPSC were only used to gain first insight into the functionality of the constructs. Further research will be performed with transduced DPSC which are preferred due to their permanent expression of the suicide gene, in contrast to the transient expression gained through transfection. Moreover, no major obstacles should occur in the transduction process, since the group of Gandia et al. showed stable transduction of GFP into DPSC, which implies that transduction of those cells is possible (66).

Recently, the interest in applying stem cells, more specifically the MSC, as a vehicle in suicide gene therapy is substantially emerging due to their better safety profile compared to viral gene delivery methods (64, 67). In this approach, the stem cells are engineered *in vitro* bearing a great potential to abolish the limitation concerning cell tracking of the viral systems on a clinical level (67, 68). Furthermore, Leten et al. provided evidence suggesting the HSV1-TK/GCV system as a possible safety switch in stem cell therapies to eliminate cells causing undesired or unrestrained effects, re-enforcing the safety profile of therapy

even more (64). However, gaining more insights and a better understanding of effectiveness and mechanism of this application is necessary. As described earlier, DPSC have several advantages compared to traditional bone marrow-derived MSCs, such as their easy isolation. Moreover, *in vitro* DPSC tropism towards the OSCC cell line and other cancer cell lines was already previously demonstrated (40).

Several considerations need to be taken into account. The first issue concerning this research can be assigned to the smaller number of technical and biological repeats of each experiment. Therefore, the sample size of all experiments should be increased in future research to strengthen and validate our results. Moreover, usage of transduced DPSC would be preferred over transfected ones since the effect of the latter is transient and time-restricted. However, the production of transduced DPSC is in its final phase; thus future experiments can be conducted with DPSC persistently expressing HSV1-TK or eGFP. Lastly, to this point, only visual observations were made concerning the expression of various markers and the occurrence of cell death. Acquiring quantitative data along with the proper statistical analysis could give a more objective overview of the obtained data.

In future research, it is of great value to enhance and expand the promising preliminary data acquired in this study to validate the stem cell-based suicide gene therapy *in vitro*. Therefore, additional analysis of gap junction formation and communication is needed to establish DPSC-OSCC GJIC as the mechanism of action of this therapy. First, ultrastructural examination of gap junction formation could strengthen the Cx43 findings and reinforce the presence of gap junction channels in the co-culture model. Transmission electron microscopy (TEM) could be employed to examine cellular interactions on this level. Furthermore, the formation of gap junctions can be emphasized in this setup in combination with immuno-gold labeling of Cx43. To reinforce GJIC as the mechanism of action, gap junction blockers (e.g. carbenoxolone or Gap27) will be used to impede this communication method (69, 70). When no dye transfer occurs in this setting, this can strengthen our other findings supporting the occurrence of gap junctional communication in the *in vitro* co-culture model.

Primary GCV cytotoxicity assays will be validated and expanded by monitoring the whole process in real-time using the Incucyte S3 (Sartorius). This will be tested on HSV1-TK-expressing DPSC, and later on the co-culture model. Optimization of this experiment is necessary to determine the GCV dosage and acquire more insight into the effect of repeated exposure to GCV. Additionally, the proper DPSC/OSCC ratio needs to be determined to eliminate all cells *in vitro*. Besides only visually observing cell death through a decrease in cell density, apoptosis can be visualized with various techniques. An Annexin V/Propidium Iodide apoptosis assay could be performed to accurately observe cell death via an improved protocol by Rieger et al. (71). Li et al. examined GCV sensitivity via an 3-(4,5)-dimethylthiahiazo-(-z-y1)-3,5-di-phenytetrazoliumromide (MTT) colorimetric assay as well as an Hoechst-propidium iodide (PI) staining (63).

To further validate the in vitro findings, *in vivo* evaluation of our proposed therapy is necessary. The animal model that will be used for this research is very translatable to the human situation and is already being established. Additional information about the generation and characterization is provided in the Supplementary section. To observe the *in vivo* potency of DPSC as a vehicle of the suicide gene therapy, they will be administered intratumorally at first. Furthermore, both the dosage of GCV and number of injected stem cells need to be evaluated in the *in vivo* settings. The ideal administration route of both DPSC and GCV needs to be assessed. Therefore, several methods will be evaluated. Later, side effects due to the therapy, such as its toxicity, need to be investigated, as well as the presence or absence of metastases.

CONCLUSION

In conclusion, our results indicate the presence of GJIC between DPSC and OSCC in an *in vitro* context. Additional gap junction blocker experiments can strengthen these findings. Based on these data, we propose GJIC as the mechanism of action responsible for the bystander effect in our stem cell-based suicide gene therapy. Furthermore, promising findings obtained from our pilot experiments support the functionality of the HSV1-TK construct and indicate GCV cytotoxicity in a dose-dependent manner. Nevertheless, since we only used transfected cells in this study, further research involving transduced DPSC is essential to evaluate their potency as vehicle for the suicide gene therapy. However, this study elucidates promising insight into both the functionality of our in-house generated construct and the bystander mechanism of the proposed therapy.

REFERENCES

1.   Bray F, Ferlay J, Soerjomataram I, Siegel RL, Torre LA, Jemal A. Global cancer statistics 2018: GLOBOCAN estimates of incidence and mortality worldwide for 36 cancers in 185 countries. CA Cancer J Clin. 2018;68(6):394-424.

2.   Hanahan D, Weinberg RA. Hallmarks of cancer: the next generation. Cell. 2011;144(5):646-74.

3.   B.T. H. Etiology of cancer. In: B. SAD, editor. Clinical Ophthalmic Oncology Switzerland Springer, Cham; 2019.

4.   Chow LQM. Head and Neck Cancer. N Engl J Med. 2020;382(1):60-72.

5.   Johnson DE, Burtness B, Leemans CR, Lui VWY, Bauman JE, Grandis JR. Head and neck squamous cell carcinoma. Nat Rev Dis Primers. 2020;6(1):92.

6.   Du E, Mazul AL, Farquhar D, Brennan P, Anantharaman D, Abedi-Ardekani B, et al. Long-term Survival in Head and Neck Cancer: Impact of Site, Stage, Smoking, and Human Papillomavirus Status. Laryngoscope. 2019;129(11):2506-13.

7.   Markopoulos AK. Current aspects on oral squamous cell carcinoma. Open Dent J. 2012;6:126-30.

8.   Pires FR, Ramos AB, Oliveira JB, Tavares AS, Luz PS, Santos TC. Oral squamous cell carcinoma: clinicopathological features from 346 cases from a single oral pathology service during an 8-year period. J Appl Oral Sci. 2013;21(5):460-7.

9.   Chi AC, Day TA, Neville BW. Oral cavity and oropharyngeal squamous cell carcinoma--an update. CA Cancer J Clin. 2015;65(5):401-21.

10.   Cavanagh TT, Holle LM. Potential new gene therapy option with sitimagene ceradenovec for newly diagnosed patients with glioblastoma multiforme. Cancer Biol Ther. 2014;15(3):263-5.

11.   Karjoo Z, Chen X, Hatefi A. Progress and problems with the use of suicide genes for targeted cancer therapy. Adv Drug Deliv Rev. 2016;99(Pt A):113-28.

12.   Kumar SR, Markusic DM, Biswas M, High KA, Herzog RW. Clinical development of gene therapy: results and lessons from recent successes. Mol Ther Methods Clin Dev. 2016;3:16034.

13.   Morgan RA, Chinnasamy N, Abate-Daga D, Gros A, Robbins PF, Zheng Z, et al. Cancer regression and neurological toxicity following anti-MAGE-A3 TCR gene therapy. J Immunother. 2013;36(2):133-51.

14.   High KA, Roncarolo MG. Gene Therapy. N Engl J Med. 2019;381(5):455-64.

15.   Pope IM, Poston GJ, Kinsella AR. The role of the bystander effect in suicide gene therapy. Eur J Cancer. 1997;33(7):1005-16.

16.   Malekshah OM, Chen X, Nomani A, Sarkar S, Hatefi A. Enzyme/Prodrug Systems for Cancer Gene Therapy. Curr Pharmacol Rep. 2016;2(6):299-308.

17.   Kokoris MS, Black ME. Characterization of herpes simplex virus type 1 thymidine kinase mutants engineered for improved ganciclovir or acyclovir activity. Protein Sci. 2002;11(9):2267-72.

18.   van Dillen IJ, Mulder NH, Vaalburg W, de Vries EF, Hospers GA. Influence of the bystander effect on HSV-tk/GCV gene therapy. A review. Curr Gene Ther. 2002;2(3):307-22.

19.   Fischer U, Steffens S, Frank S, Rainov NG, Schulze-Osthoff K, Kramm CM. Mechanisms of thymidine kinase/ganciclovir and cytosine deaminase/ 5-fluorocytosine suicide gene therapy-induced cell death in glioma cells. Oncogene. 2005;24(7):1231-43.

20.   Adachi M, Sampath J, Lan LB, Sun D, Hargrove P, Flatley R, et al. Expression of MRP4 confers resistance to ganciclovir and compromises bystander cell killing. J Biol Chem. 2002;277(41):38998-9004.

21.   Ardiani A, Johnson AJ, Ruan H, Sanchez-Bonilla M, Serve K, Black ME. Enzymes to die for: exploiting nucleotide metabolizing enzymes for cancer gene therapy. Curr Gene Ther. 2012;12(2):77-91.

22.   Black ME, Kokoris MS, Sabo P. Herpes simplex virus-1 thymidine kinase mutants created by semi-random sequence mutagenesis improve prodrug-mediated tumor cell killing. Cancer Res. 2001;61(7):3022-6.

23.   Candice LW, Django S, Margaret EB. The role of herpes simplex virus-1 thymidine kinase alanine 168 in substrate specificity. Open Biochem J. 2008;2:60-6.

24.   Nicholas TW, Read SB, Burrows FJ, Kruse CA. Suicide gene therapy with Herpes simplex virus thymidine kinase and ganciclovir is enhanced with connexins to improve gap junctions and bystander effects. Histol Histopathol. 2003;18(2):495-507.

25.   Mesnil M, Yamasaki H. Bystander effect in herpes simplex virus-thymidine kinase/ganciclovir cancer gene therapy: role of gap-junctional intercellular communication. Cancer Res. 2000;60(15):3989-99.

26.   Zarogoulidis P, Darwiche K, Sakkas A, Yarmus L, Huang H, Li Q, et al. Suicide Gene Therapy for Cancer - Current Strategies. J Genet Syndr Gene Ther. 2013;4.

27.   Mohit E, Rafati S. Biological delivery approaches for gene therapy: strategies to potentiate efficacy and enhance specificity. Mol Immunol. 2013;56(4):599-611.

28.   Laird DW. Life cycle of connexins in health and disease. Biochem J. 2006;394(Pt 3):527-43.

29.   Sohl G, Willecke K. Gap junctions and the connexin protein family. Cardiovasc Res. 2004;62(2):228-32.

30.   Brockmeyer P, Jung K, Perske C, Schliephake H, Hemmerlein B. Membrane connexin 43 acts as an independent prognostic marker in oral squamous cell carcinoma. Int J Oncol. 2014;45(1):273-81.

31.   Miletic H, Fischer Y, Litwak S, Giroglou T, Waerzeggers Y, Winkeler A, et al. Bystander killing of malignant glioma by bone marrow-derived tumor-infiltrating progenitor cells expressing a suicide gene. Mol Ther. 2007;15(7):1373-81.

32.   Martens W, Wolfs E, Struys T, Politis C, Bronckaers A, Lambrichts I. Expression pattern of basal markers in human dental pulp stem cells and tissue. Cells Tissues Organs. 2012;196(6):490-500.

33.   Didilescu AC, Rusu MC, Nini G. Dental pulp as a stem cell reservoir. Rom J Morphol Embryol. 2013;54(3):473-8.

34.   Leeb C, Jurga M, McGuckin C, Moriggl R, Kenner L. Promising new sources for pluripotent stem cells. Stem Cell Rev Rep. 2010;6(1):15-26.

35.   Zakrzewski W, Dobrzynski M, Szymonowicz M, Rybak Z. Stem cells: past, present, and future. Stem Cell Res Ther. 2019;10(1):68.

36.   Kim HJ, Park JS. Usage of Human Mesenchymal Stem Cells in Cell-based Therapy: Advantages and Disadvantages. Dev Reprod. 2017;21(1):1-10.

37.   Dominici M, Le Blanc K, Mueller I, Slaper-Cortenbach I, Marini F, Krause D, et al. Minimal criteria for defining multipotent mesenchymal stromal cells. The International Society for Cellular Therapy position statement. Cytotherapy. 2006;8(4):315-7.

38.   Andrukhov O, Behm C, Blufstein A, Rausch-Fan X. Immunomodulatory properties of dental tissue-derived mesenchymal stem cells: Implication in disease and tissue regeneration. World J Stem Cells. 2019;11(9):604-17.

39.   Hilkens P, Gervois P, Fanton Y, Vanormelingen J, Martens W, Struys T, et al. Effect of isolation methodology on stem cell properties and multilineage differentiation potential of human dental pulp stem cells. Cell Tissue Res. 2013;353(1):65-78.

40.   Merckx G, Lo Monaco M, Lambrichts I, Himmelreich U, Bronckaers A, Wolfs E. Safety and Homing of Human Dental Pulp Stromal Cells in Head and Neck Cancer. Stem Cell Rev Rep. 2021.

41.   Howard C, Murray PE, Namerow KN. Dental pulp stem cell migration. J Endod. 2010;36(12):1963-6.

42.   Tiscornia G, Singer O, Verma IM. Production and purification of lentiviral vectors. Nat Protoc. 2006;1(1):241-5.

43.   Panarese I, Aquino G, Ronchi A, Longo F, Montella M, Cozzolino I, et al. Oral and Oropharyngeal squamous cell carcinoma: prognostic and predictive parameters in the etiopathogenetic route. Expert Rev Anticancer Ther. 2019;19(2):105-19.

44.   Faneca H, Duzgunes N, Pedroso de Lima MC. Suicide Gene Therapy for Oral Squamous Cell Carcinoma. Methods Mol Biol. 2019;1895:43-55.

45.   Wang Q, Gao P, Wang X, Duan Y. The early diagnosis and monitoring of squamous cell carcinoma via saliva metabolomics. Sci Rep. 2014;4:6802.

46.   Neves S, Faneca H, Bertin S, Konopka K, Duzgunes N, Pierrefite-Carle V, et al. Transferrin lipoplex-mediated suicide gene therapy of oral squamous cell carcinoma in an immunocompetent murine model and mechanisms involved in the antitumoral response. Cancer Gene Ther. 2009;16(1):91-101.

47.   Chen LS, Wang M, Ou WC, Fung CY, Chen PL, Chang CF, et al. Efficient gene transfer using the human JC virus-like particle that inhibits human colon adenocarcinoma growth in a nude mouse model. Gene Ther. 2010;17(8):1033-41.

48.   Duarte S, Carle G, Faneca H, de Lima MC, Pierrefite-Carle V. Suicide gene therapy in cancer: where do we stand now? Cancer Lett. 2012;324(2):160-70.

49.   Lin CS, Xin ZC, Dai J, Lue TF. Commonly used mesenchymal stem cell markers and tracking labels: Limitations and challenges. Histol Histopathol. 2013;28(9):1109-16.

50.   Coulombe PA, Omary MB. 'Hard' and 'soft' principles defining the structure, function and regulation of keratin intermediate filaments. Curr Opin Cell Biol. 2002;14(1):110-22.

51.   Alix-Panabieres C, Vendrell JP, Slijper M, Pelle O, Barbotte E, Mercier G, et al. Full-length cytokeratin-19 is released by human tumor cells: a potential role in metastatic progression of breast cancer. Breast Cancer Res. 2009;11(3):R39.

52.   Rajeswari P, Janardhanan M, Suresh R, Savithri V, Aravind T, Raveendran GC. Expression of CK 19 as a biomarker in early detection of oral squamous cell carcinoma. J Oral Maxillofac Pathol. 2020;24(3):523-9.

53.   MUJYAMBERE BONAVENTURE JR, S S. . Cytokeratin 19 (CK19) as a marker for Epithelial Differentiation and Malignant Transformation: Its Clinical relevance in Diagnosis, Prognosis and Treatment response monitoring. IRE Journals 2018;2(3):11.

54.   Luzuriaga J, Pineda JR, Irastorza I, Uribe-Etxebarria V, Garcia-Gallastegui P, Encinas JM, et al. BDNF and NT3 Reprogram Human Ectomesenchymal Dental Pulp Stem Cells to Neurogenic and Gliogenic Neural Crest Progenitors Cultured in Serum-Free Medium. Cell Physiol Biochem. 2019;52(6):1361-80.

55.   Hanani M. Lucifer yellow - an angel rather than the devil. J Cell Mol Med. 2012;16(1):22-31.

56.   Dydowiczova A, Brozman O, Babica P, Sovadinova I. Improved multiparametric scrape loading-dye transfer assay for a simultaneous high-throughput analysis of gap junctional intercellular communication, cell density and viability. Sci Rep. 2020;10(1):730.

57.   Abbaci M, Barberi-Heyob M, Blondel W, Guillemin F, Didelon J. Advantages and limitations of commonly used methods to assay the molecular permeability of gap junctional intercellular communication. Biotechniques. 2008;45(1):33-52, 6-62.

58.   Ragnarson B, Bengtsson L, Haegerstrand A. Labeling with fluorescent carbocyanine dyes of cultured endothelial and smooth muscle cells by growth in dye-containing medium. Histochemistry. 1992;97(4):329-33.

59.   CellMask™ Plasma Membrane Stains. In: ThermoFisher, editor.: Molecular probes by life technologies; 2014.

60.   Hoffmann J, Mendgen K. Endocytosis and membrane turnover in the germ tube of uromyces fabae. Fungal Genet Biol. 1998;24(1-2):77-85.

61.   Tech Tip: Using ViaFluor® SE Stains for Cell Tracing and Co-Culture: Biotium; [Available from: https://biotium.com/tech-tips/tech-tip-using-viafluor-se-stains-for-cell-tracing-and-co-culture/.

62.   Weber EL, Cannon PM. Promoter choice for retroviral vectors: transcriptional strength versus trans-activation potential. Hum Gene Ther. 2007;18(9):849-60.

63.   Li LQ, Shen F, Xu XY, Zhang H, Yang XF, Liu WG. Gene therapy with HSV1-sr39TK/GCV exhibits a stronger therapeutic efficacy than HSV1-TK/GCV in rat C6 glioma cells. ScientificWorldJournal. 2013;2013:951343.

64.   Leten C, Roobrouck VD, Struys T, Burns TC, Dresselaers T, Vande Velde G, et al. Controlling and monitoring stem cell safety in vivo in an experimental rodent model. Stem Cells. 2014;32(11):2833-44.

65.   Liu Z, Chen O, Wall JBJ, Zheng M, Zhou Y, Wang L, et al. Systematic comparison of 2A peptides for cloning multi-genes in a polycistronic vector. Sci Rep. 2017;7(1):2193.
66.   Gandia C, Arminan A, Garcia-Verdugo JM, Lledo E, Ruiz A, Minana MD, et al. Human dental pulp stem cells improve left ventricular function, induce angiogenesis, and reduce infarct size in rats with acute myocardial infarction. Stem Cells. 2008;26(3):638-45.
67.   Kim JH, Lee HJ, Song YS. Stem cell based gene therapy in prostate cancer. Biomed Res Int. 2014;2014:549136.
68.   Pulkkanen KJ, Yla-Herttuala S. Gene therapy for malignant glioma: current clinical status. Mol Ther. 2005;12(4):585-98.
69.   Manjarrez-Marmolejo J, Franco-Perez J. Gap Junction Blockers: An Overview of their Effects on Induced Seizures in Animal Models. Curr Neuropharmacol. 2016;14(7):759-71.
70.   Evans WH, Leybaert L. Mimetic peptides as blockers of connexin channel-facilitated intercellular communication. Cell Commun Adhes. 2007;14(6):265-73.
71.   Rieger AM, Nelson KL, Konowalchuk JD, Barreda DR. Modified annexin V/propidium iodide apoptosis assay for accurate assessment of cell death. J Vis Exp. 2011(50).

Author contributions – E.W. conceived and designed the project and the associated theoretical frame work. E.W. and J.VDB. supervised the study. K.N. and J.VDB. were involved in the daily planning of the project. K.N. and J.VDB. performed experiments and data analysis. J.VDB. conducted the Lucifer Yellow dye transfer assay, whereby assistance was provided by Petra Bex for cell-patching. J.VDB supplied the lentiviral particles required for DPSC transduction, K.N. followed along with this process. K.N. wrote the manuscript and designed the figures with support from J.VDB. E.W. and J.VDB. reviewed the final paper. All authors carefully edited the manuscript.

SUPPLEMENTARY INFORMATION
A. SUPPLEMENTARY TABLES

Suppl. Table 1 – Abbreviation list	
Abbreviation	
α-MEM	Alfa-modification of minimum essential medium
AmpR	Ampicillin resistant cassette
BLI	Bioluminescence imaging
BM-MSC	Bone marrow-derived mesenchymal stem cells
Ck	Cytokeratin
CMR	Cell mask deep red
Cx43	Connexin 43
DAB	3,3'-Diaminobenzidine
DAPI	4',6-diamidino-2-phenylindole
DMEM	Dulbecco's modified eagle medium
DiI	1,1'-Dilinoleyl-3,3,3',3'-Tetramethylindocarbocyanine Perchlorate
EBV	Ebstein Barr Virus
HEK293T	Human Embryonic Kidney cell line 293T
HI-FCS	Heat inactivated Fetal calf serum
E. coli	*Escherichia* coli
EF1a	Human elongation factor-1 alpha
Fluc	Firefly luciferase
GCV	Ganciclovir (Cymevene)
GDEPT	Gene-directed enzyme prodrug therapy
GFP	Green fluorescent protein
GJIC	Gap junction intercellular communication
DPSC	Human dental pulp stem cell
HNC	Head and neck squamous cell carcinoma
HPV	Human Papilloma Virus
HSV1-TK	Herpes Simplex Virus 1 – Thymidine kinase
IRES	Internal ribosome entry site
ISCT MSC	International Society for Cellular Therapy Mesenchymal and Tissue Stem Cell Committee
LM	Light microscopy
MSC	Mesenchymal stem cell
MTT	3-(4,5)-dimethylthiahiazo-(-z-y1)-3,5-di-phenytetrazoliumromide
OSCC	Oral squamous cell carcinoma
PI	Propidium Iodide
P/S	Penicillin/streptomycin
PBS	Phosphate buffered saline
RT	Room temperature
T2A	Peptide 2A
TEM	Transmission electron microscopy
ZOL	Ziekenhuis Oost-Limburg

Suppl. Table 2 – Restriction enzyme used in the cloning process.

Restriction enzymes	Cutting site	Company
FD-EcorI	5' G↓A A T T C 3' 3' C T T A A↑G 5'	Thermo Fisher Scientific Ref.: FD0274
FD-MssI	5' G T T T↓A A A C 3' 3' C A A A↑ T T T G 5'	Thermo Fisher Scientific Ref.: FD1344
FD-XbaI	5' T↓C T A G A 3' 3' A G A T C↑T 5'	Thermo Fisher Scientific Ref.: FD0684
FD-NdeI	5' C A↓T A T G 3' 3' G T A T↑A C 5'	Thermo Fisher Scientific Ref.: FD0583
FD-BcuI	5' A↓C T A G T 3' 3' T G A T C↑A 5'	Thermo Fisher Scientific Ref.: FD1253
FD-MreI	5' C G↓C C G G C G 3' 3' G C G G C C↑G C 5'	Thermo Fisher Scientific Ref.: FD2024

FD; Fast Digest

Suppl. Table 3| Detailed overview of the primary antibodies used for ICC and IHC.

| Target	Primary AB				
	Species	Type	Dilution	Reference nr.	Manufacturer
CD105	Mouse IgG1	Monoclonal	1:100	8000501	Biolegend (Amsterdam, The Nederlands)
Connexin-43	Rabbit IgG	Polyclonal	1:1000	ab11370	Abcam (Leuven, Belgium)
Cytokeratin MNF116	Mouse IgG	Monoclonal	1:100	M0821	Dako (Heverlee, Belgium)
Flag-tag	Mouse IgG1	Monoclonal	1:500	F1804	Sigma-Aldrich (Overijse, Belgium)
GFP	Rabbit IgG	Polyclonal	1:200	ab290	Abcam (Leuven, Belgium)
His-tag	Mouse IgG2b	Monoclonal	1:500	MA1-21315	Invitrogen (Merelbeke, Belgium)
HSV1-TK	Rabbit	Monoclonal	1:500	YO53063	Gentaur (Kampenhout, Belgium)
Ki67	Rabbit IgG	Polyclonal	1:500	ab15580	Abcam (Leuven, Belgium)
MAGE-A3	Rabbit	Polyclonal	1:250	SAB2101419	Sigma-Aldrich (Overijse, Belgium)
p63	Rabbit	Monoclonal	1:200	ab124762	Abcam (Leuven, Belgium)

CD105; endoglin, GFP; Green Fluorescent Protein, HSV1-TK; Herpes Simplex Virus 1 Thymidine Kinase, Ki67; Marker of Proliferation Ki67, MAGE-A3; melanoma-associated antigen 3, p63; tumor protein p63

Suppl. Table 4| Detailed overview of the secondary antibodies used for ICC and IHC.					
	Secondary Antibody				
	Species	**Reactivity**	**Dilution**	**Reference nr.**	**Manufacturer**
Alexa Fluor 488	Goat IgG1	Anti-mouse	1:200	A21121	Invitrogen (Merelbeke, Belgium)
Alexa Fluor 555	Donkey IgG (H+L)	Anti-rabbit	1:200	A31572	Invitrogen (Merelbeke, Belgium)
		Anti-mouse	1:200	A31570	
HRP-labeled	Goat IgG	Anti-rabbit	1:200	P0448	Dako (Heverlee, Belgium)
HRP; Horseradish peroxidase, IgG; Immunoglobulin G, H+L; Heavy and light chain					

## B. SUPPLEMENTARY FIGURES
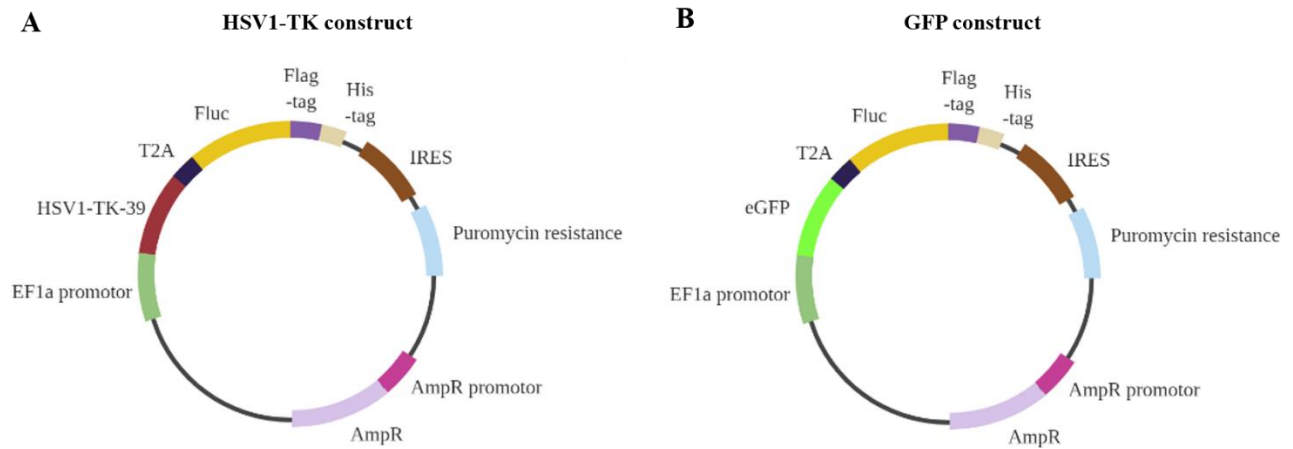
Suppl. Fig. 1| The transfer plasmids expressing Herpes Simplex Virus 1 thymidine kinase (HSV1-TK) and enhanced Green Fluorescent Protein (eGFP) were successfully engineered. Both constructs were generated by cloning the insert containing, among others, the gene of interest into an in-house generated pSin vector. Each construct contained an human elongation factor-1 alpha (EF1a) promotor to drive the gene expression and was designed to express **(A)** HSV1-TK or **(B)** eGFP linked to a Flag- and His-tagged Firefly Luciferase (FLuc) and puromycin resistance cassette via a peptide 2A (T2A) sequence and internal ribosome entry site (IRES), respectively. Additionally, ampicillin resistance (AmpR) was also included in each transfer plasmid.

C. CHARACTERIZATION OF THE 4NQO ANIMAL MODEL

Rats and treatment protocol – Wistar rats were purchased from Janvier Labs to optimize the 4-nitroquinoline-1-oxide (4NQO) animal model. All animal experiments were performed according to guidelines and approved by the Ethical Committee of Hasselt University. Rats were divided into four groups, with each group receiving a different treatment. 4NQO, a carcinogenic substance present in tobacco, was dissolved in propylene glycol and administered either within the rat's drink water (0.1 mg/mL, n=27) or directly on its tongue (5mg/mL, 3x/week n =27). Propylene glycol only was applied onto the tongue of the first control group (n=3) to exclude any effect of the 4NQO-dissolving solution. The second control group received no treatment (negative control, n=3). To determine the exact timeframe in which tumor formation occurred, rats were sacrificed each month starting from two months into treatment, control animals were sacrificed at the end point of this in vivo experiment. Afterward, the tongues were dissected, and the tissue was processed and embedded in paraffin.

Histopathological examination of the tongue tissue – The paraffine-embedded tissue was deparaffinized prior to conducting the Masson's Trichrome or immunohistochemistry (IHC) staining. First, Masson's Trichome staining was performed to generate an overview of the tissue's general histology. The tissue was first stained with Meyer's Hematoxylin to visualize the nuclei (dark brown). Next, to distinguish the cytoplasm and muscle tissue, sections were stained by a Ponceau-Fuchsin solution. Lastly, Aniline blue was used to visualize any collagen (blue) present in the tissue sections. Furthermore, IHC stainings (Representative images in **Suppl. Fig. 2**) were conducted to assess the expression of three commonly used cancer diagnostic markers: a marker of proliferation Ki67 (Ki67; **Suppl. Fig. 2B**), tumor protein p63 (p63; **Suppl. Fig. 2C**), and Melanoma-associated antigen 3 (MAGE-A3; **Suppl. Fig. 2D**). First, antigen retrieval was achieved by a 30 min incubation of the tissue sections in boiling citric acid buffer. Subsequently, endogenous peroxidase activity was neutralized by adding a peroxidase block solution (30% H_2O_2 (Dako) in methanol; 1:10 ratio) for 25 min. Non-specific binding was avoided by a 30 min 10% protein block prior to the overnight incubation of the proper primary antibody (Supplementary Table 3) at 4°C. The next day, a suitable HRP-labeled secondary antibody (Supplementary Table 4) was incubated for 30 min, followed by the addition of the Liquid DAB⁺ Substrate Chromogen System (Dako, K3468) for a maximum of 8 min. Subsequently, Meyer's Hematoxylin was used as a counterstaining. After finalizing each staining, the tissue sections were dehydrated and mounted with DPX. The AxioScan.Z1 (ZEISS) and Zen 3.2 (Blue edition, ZEISS) software were used to visualize the stained tissue sections. Analysis was performed by a specialized pathologist and radiologist to determine the best method (time point and treatment condition) to create the 4NQO animal model.
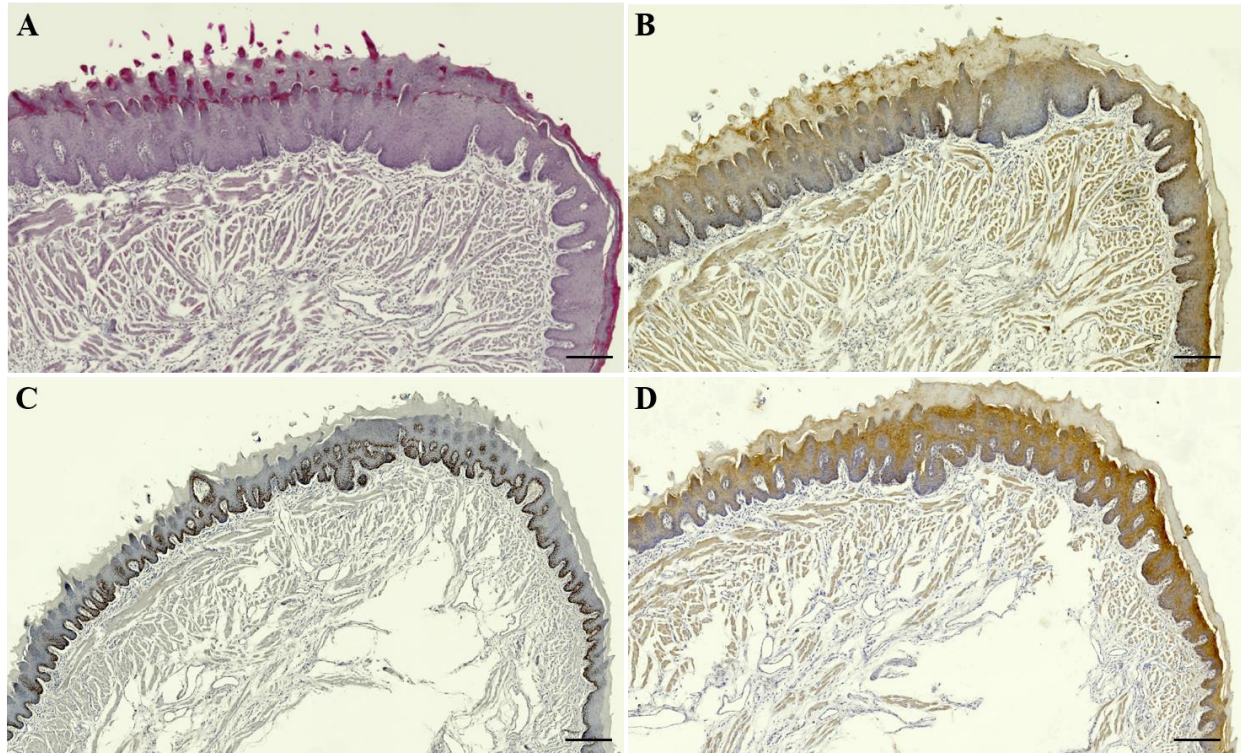
Suppl. Fig. 2| Masson's trichome staining and immunohistochemistry (IHC) of tongues obtained from the 4-nitroquinoline-1-oxide (4NQO) rat model. The presented tissue was obtained from a rat treated for four months with 4NQO directly applied on its tongue. **(A)** Masson's trichrome staining provides an histological overview of the tongue tissue. **(B-D)** IHC analysis was performed to visualize the expression of several markers – **(B)** Ki67, **(C)** p63, **(D)** MAGEA3 - also used in a clinical setting to evaluate tissue biopsy. Figure shown as illustration of ongoing characterization of the animal model. Scalebar = **(A, B, D)** 200 µm, **(C)** 500µm